Correspondence to:

L. G. Silvers,
levi.silvers@stonybrook.edu

Clouds and Radiation in a Mock-Walker Circulation

Levi G. Silvers[1,3] , and **Thomas Robinson[2]**

[1]Princeton University/GFDL, Princeton, NJ, USA, [2]NOAA/GFDL, SAIC, Science Applications International Corporation, Reston, VA, USA, [3]School of Marine and Atmospheric Sciences, Stony Brook University, Stony Brook, NY, USA

Abstract The Walker circulation connects the regions with deep atmospheric convection in the western tropical Pacific to the shallow-convection, tropospheric subsidence, and stratocumulus cloud decks of the eastern Pacific. The purpose of this study is to better understand the multi-scale interactions between the Walker circulation, cloud systems, and interactive radiation. To do this we simulate a mock-Walker Circulation with a full-physics general circulation model using idealized boundary conditions. Our experiments use a doubly-periodic domain with grid-spacing of 1, 2, 25, and 100 km. We thus span the range from General Circulation Models (GCMs) to Cloud-system Resolving Models (CRMs). Our model is derived from the Geophysical Fluid Dynamics Laboratory atmospheric GCM (AM4.0). We find substantial differences in the mock-Walker circulation simulated by our GCM-like and CRM-like experiments. The CRM-like experiments have more upper level clouds, stronger overturning circulations, and less precipitation. The GCM-like experiments have a low-level cloud fraction that is up to 20% larger. These differences leads to opposite atmospheric responses to changes in the longwave cloud radiative effect (LWCRE). Active LWCRE leads to increased precipitation for our GCMs, but decreased precipitation for our CRMs. The LWCRE leads to a narrower rising branch of the circulation and substantially increases the fraction of precipitation from the large-scale cloud parameterization. This work demonstrates that a mock-Walker circulation is a useful generalization of radiative convective equilibrium that includes a large-scale circulation.

Plain Language Summary Interactions between clouds, radiation, and dynamics all contribute to the large-scale tropical motions and are fundamental to the Walker circulation. The Walker circulation is a loop consisting of surface winds toward the western tropical Pacific, strong upward motion and deep convection in that region, and the return eastward winds aloft that eventually sink toward the surface in the eastern Pacific basin. We focus on an idealization of the Walker circulation (a mock-Walker circulation) in which the strong rising motion and deep convection is driven by a patch of warm sea surface temperature. Our results show that the response of the atmosphere to the radiative flux of energy depends strongly on the relative amount of clouds at different heights. It is further shown that our GCM-like models are dominated by low-clouds while our CRM-like models are dominated by high-clouds. This work also argues that an idealized Walker circulation is an excellent configuration with which to better understand the interactions between clouds, radiation, and circulation and to push the development of models forward. Models of mock-Walker circulations represent an intermediate tier in a hierarchy of models between Earth-like models and models of radiative convective equilibrium.

1. Introduction

The tropical Pacific is an ideal location to study interactions between clouds and the circulation because it combines strong overturning circulations, abundant shallow cumulus, congestus, and cumulonimbus clouds (Johnson et al., 1999) as well as stratocumulus cloud decks along the eastern extremities of the basin. These overturning circulations encompass dynamical motions at scales ranging from meters to thousands of kilometers all of which interact with each of the different cloud types. The circulation first noted by Sir Gilbert Walker, and described by Bjerknes (1969) connects the western Pacific region with warm sea surface temperature (SST) and strong deep convection to the eastern Pacific region which tends to be populated more by shallow cumulus and, in the subtropics, stratocumulus clouds. This circulation, now known as the Walker Circulation, is a response to longitudinal asymmetries in tropical atmospheric heating and is tightly

coupled with the El Niño-Southern Oscillation (ENSO). The Walker Circulation is composed of both thermodynamic and dynamic interactions between moisture and the large-scale circulation. As such, it provides an excellent example with which to analyze the overturning circulation and interactions between clouds and radiation using a variety of model configurations.

It is also clear that the tropical Pacific plays an important role in the response of the climate to radiative perturbations. Recent work has shown that the interactions between clouds, patterns of SST, and the circulation in the tropical Pacific play an important role in determining the cloud feedback and the decadal variability of the climate feedback (e.g., Andrews & Webb, 2018; Fueglistaler, 2019; Silvers et al., 2018; Zhou et al., 2016). While the Hadley circulation connects the tropics with the midlatitudes, the Walker circulation is one of the primary mechanisms by which the clouds, SST, and circulations are coupled to each other in the tropics. We propose that focusing on the Walker Circulation can lead to new insights into several questions that are critical to a better understanding of tropical climate and cloud processes. These questions include:

- How do clouds influence the overturning circulation?
- To what extent are deep convective clouds and low-level clouds coupled through overturning circulations?
- When simulating tropical overturning circulations, how well does a GCM compare to a CRM?

In global and Earth-like GCM simulations, the interplay between the overturning circulation and clouds is difficult to disentangle from other processes such as the Hadley cell and convectively coupled tropical waves. Many of the studies with Cloud-system Resolving Models (CRMs) that have focused on the tropical overturning circulation in a more idealized context have been restricted to relatively small domain sizes and highly simplified physics parameterizations. The result is a gap in the types of simulation for this region that is so important to our understanding of clouds in the Earth's climate system.

This work uses the framework of a mock-Walker circulation to simulate an overturning tropical circulation with both a GCM-like model and a CRM-like model. Idealized models of the Walker circulation were referred to as 'mock-Walker circulations' by Raymond (1994). Raymond (1994) envisioned an idealized Walker circulation as, "a possible venue for testing ideas about the interaction of dynamics, moist convection, and sea-air transfers that is simple enough to be understandable, but rich enough to be interesting." Using the mock-Walker circulation as a tool to help distill the processes in complex climate models into concrete understanding was also proposed by Jeevanjee et al. (2017). There have been many notable studies of the Walker Circulation (e.g., Bretherton & Sobel, 2002; Bretherton et al., 2006; Geisler, 1981; Grabowski et al., 2000; Raymond, 1994; Schwendike et al., 2014; Tompkins, 2001; Wofsy & Kuang, 2012). Previous studies have focused on observations (Bjerknes, 1969; Schwendike et al., 2014), theory (Bretherton & Sobel, 2002; Geisler, 1981; Gill, 1980; Iipponen & Donner, 2020; Raymond, 1994), or a combination of modeling and simple theory (Bretherton et al., 2006; Grabowski et al., 2000; Kuang, 2012; Peters & Bretherton, 2005; Sobel et al., 2004; Wofsy & Kuang, 2012). The modeling studies have primarily used models we refer to as Cloud-system Resolving Models (CRMs; grid-spacing of less than 5 km, no convective parameterization). Multiple studies have presented elegant conceptual and theoretical models of the overturning tropical circulation (Bretherton & Sobel, 2002; Larson et al., 1999; Pierrehumbert, 1995; Raymond, 1994). However, these simplified theoretical models of the circulation differ from each other in important details and have different parameter dependencies. Their simplicity helps to provide insight into those models, but is difficult to translate to the tropical climates produced by GCMs. Most of these previous studies greatly simplify both the radiation and the representation of clouds. They point to the importance of the interactions between clouds, radiation, and the large-scale circulation while avoiding much of the complexity of those processes.

Current climate models continue to be developed with an increasingly fine resolution and the domain sizes used with CRMs continues to grow. The parameter space of GCMs and CRMs has begun to overlap but the representation of physics continues to differ by much more than grid-spacing and the treatment of convection. As a result there is a need to systematically compare the clouds and their influence on the climate produced by each type of model (Schneider et al., 2017). By simulating a mock-Walker Circulation in the context of both a GCM and a CRM that have been derived from the same model, we illustrate how inextricable the interactions between clouds and radiation are to the coupling of moisture with the large-

scale circulation. The model used here is based on the Geophysical Fluid Dynamics Laboratory (GFDL) AM4.0 GCM that participated in CMIP6, having a full suite of physics parameterizations. Rather than a full global domain all of our experiments use a doubly-periodic domain. This is conceptually similar to Held et al. (2007), which used an earlier generation GFDL climate model on a doubly-periodic domain to study radiative convective equilibrium (RCE). The combination of a doubly periodic domain and a current generation climate model allow us to analyze the interactions of the circulation and clouds in simulations with grid-spacing that ranges from 1 km to 100 km. We thus study a full-physics GCM in an idealized context that is relevant to observed tropical systems, to theoretical models of tropical circulations, and to many studies of RCE.

The broad goal of this paper is to clarify the two-way interactions between the Walker circulation and the various cloud types that are prevalent in the tropical Pacific. Our specific goal is to compare the Walker circulation and clouds simulated with a GCM-like model to analogous simulations from a CRM-like model using one modeling framework based on a single code base. This serves as the framework with which we naively attempt to transition a GCM toward a CRM. By simulating a tropical Pacific-like region in GCM-like and CRM-like models, we are able to better understand the physics and the mechanisms which are at work in the cloud-circulation interactions of the tropical Pacific and improve our ability to model this region in a GCM. We perform a series of sensitivity experiments that highlight the different ways in which these experiments can equilibrate. The climatology of the precipitation, both the amount and location, is particularly sensitive to changes in the configuration. We demonstrate the impact to the mean state of convective parameterization, LW radiative interactions with clouds, domain size, and the resolution, or grid-spacing.

The paper is organized as follows. Details of the model and the particular experiments used are described in the next section. Section three gives a broad description of the mock-Walker circulation in our simulations and describes the tendency of experiments with parameterized convection to settle into states which do not mirror the symmetry of the prescribed SST. Then, section four shows how the distribution of precipitation changes as a function of domain size. Section five will describe and contrast the Walker circulation in a GCM-like and a CRM-like configuration. Section six includes a summary of our results and a brief discussion. The longwave cloud radiative effect (LWCRE) is an important element for all of the experiments and will be discussed throughout the paper.

2. Experimental Details and Methods

All simulations use a nonhydrostatic dynamical core, with prescribed SSTs and a doubly periodic domain which is elongated in the zonal direction allowing for three dimensional simulations but with a reduced computational cost relative to the default global domain. The domain is flat, non-rotating, and has uniform and constant insolation. The lower boundary is a water covered surface with the SST prescribed as a time invariant Gaussian function which is 4K warmer in the center (301 K/27.85 C) of the domain than at the edges (297K/23.85 C). To develop the model configuration used for these experiments we started with the same code base as that of the recently developed atmospheric global climate model AM4.0 (Zhao et al., 2018a, 2018b) (Z18a and Z18b hereafter). AM4.0 uses the GFDL finite-volume cubed-sphere dynamical core FV3 (Harris & Lin, 2013) which can solve either the hydrostatic primitive equations or the nonhydrostatic fully compressible Euler equations over a wide range of resolutions. Current generation global GFDL models use a cubed-sphere grid composed of six tiles. We use the model on a single doubly-periodic tile. This allows the grid-spacing and domain size to be easily changed to minimize the cost of computations. This study focuses on experiments with grid-spacing of 1, 2, 25, and 100 km on several different sizes of domain. Additional details are given in Table 1.

The default AM4.0 physics we use include interactive radiation, parameterized deep- and shallow-convection, a large-scale cloud scheme, and a boundary layer scheme as described in Z18a, b, and the references therein. The prognostic moisture variables are the specific humidity (q), liquid (ql), frozen water (qi), and cloud fraction. The top of the model domain is at 1 hPa, with 33 vertical levels and a sponge layer extending downward to 8 hPa. The kilometer of atmosphere just above the surface is resolved by eight model levels. Changes made to the default AM4.0 physics in this study are as follows. The cloud-aerosol interactions were turned off to focus on the interaction between clouds, radiation, and the circulation. The gravity wave drag

Table 1
Specifications of the Experiments Used Most Heavily in This study

Name	Grid spacing (km)	dt (s)	Domain (km^2)	Length (months)	Convection
P100 L	100	600	800 × 16,000	60	prm
P100	100	600	800 × 4,000	60	prm
P25 L	25	600	200 × 16,000	60	prm
P25	25	600	200 × 4,000	60	prm
E25	25	600	200 × 4,000	60	expl
E2	2	20	100 × 4,000	6	expl
E1	1	5	10 × 4,000	6	expl

Note. The length of computational time step is represented by 'dt'. In the Convection column, 'prm' indicates that convection is parameterized and 'expl' indicates explicit convection. All of the experiments listed here were also run with the LWCRE turned off and are referred to with a LWCRE-off suffix in the text. For example, P100 L LWCRE-off, etc.

parameterization was turned off in order to reduce large oscillations which developed in the horizontal wind field near the top of the model domain. The convection, radiation, large-scale cloud, microphysics, and turbulence parameterizations all remain the same as in AM4.0. Thus for the experiments with the convection parameterized (grid-spacing of 25 and 100 km), the physics are very similar to those of AM4.0. This configuration of AM4.0 physics was initially used by Popp and Silvers (2017) and more recently for the aquaplanet model used as part of GFDL's contribution to the Cloud Feedback Model Intercomparison Project (CFMIP) component of CMIP6.

One of the ways in which clouds influence the flow of energy through the atmosphere is by absorbing and reemitting longwave radiation. A technique that has been commonly used to infer the influence of clouds on the atmospheric mean state is to make the clouds invisible to the radiation. The usual two-way interaction between clouds and radiation is thus broken and a useful diagnostic tool is created. This method was originally pioneered by Slingo and Slingo (1988) and Randall et al. (1989). More recently, it has been implemented as part of the CFMIP series of experiments (Stevens et al., 2012; Webb et al., 2017). Another technique, referred to as "cloud-locking," can be used to infer how interactions between clouds, radiation, and circulation influence the climate variability (e.g., Radel et al., 2016). This method allows one to decouple the cloud radiative effect from the atmospheric state by holding clouds from a control experiment fixed while the rest of the experiment responds to some perturbation. This paper does not use the "cloud-locking" method. In the AM4 code, we make the clouds invisible to the radiation separately for the longwave (LW) and shortwave radiation. In this study, we compare control experiments, in which clouds and radiation are fully interactive, with experiments in which clouds are invisible to the LW radiation. These experiments are referred to as Longwave Cloud Radiative Effect Off (LWCRE-off). Clouds also interact with shortwave radiation. We have chosen to only focus on the LWCRE for several reasons. On timescales of years and over large domains, the LWCRE has been shown (e.g., Popp & Silvers, 2017) to have a much larger influence on the atmospheric heating and the large-scale circulations compared to the Shortwave Cloud Radiative Effect (SWCRE). The SWCRE is important on diurnal timescales and for the surface energy budget. However, we choose to leave simulations exploring the SWCRE in the context of the mock-Walker circulation for a later study. For the LWCRE-off experiments, both the LW and shortwave radiation are present and interact with the atmospheric state, the clouds still precipitate and interact with the shortwave radiation. Turning off the LWCRE would have a large impact on the surface budget of a coupled model. However, because there is no land in our simulations and the SST is held fixed, the energetics of our experiments are not as strongly affected as might be expected. Experiments with only a water surface at the lower boundary and fixed SST are an ideal configuration to utilize the LWCRE-off configuration.

The experiments with 100 and 25 km grid-spacing have been run for 5 years while the 1 and 2 km experiments were run for 6 months. Experiments with parameterized convection are labeled with a P prefix, followed by a number indicating the grid-spacing in kilometers while the experiments with explicit convection (no parameterized convection) will be labeled with an E prefix, followed by the appropriate number. Thus P25 refers to an experiment with parameterized convection using a grid-spacing of 25 km. The naming

convention for each of the experiments is shown in Table 1. Throughout this paper the P100 and P25 experiments, with and without the LWCRE, are referred to as "GCM-like" while the E2 and E1 experiments are referred to as "CRM-like." The GCM-like experiments differ from traditional GCMs in the non-global domain and lack of rotation. The CRM-like terminology acknowledges that this configuration has a vertical resolution that is coarser than many CRMs, and uses the large-scale cloud scheme from the AM4.0/CM4.0 GCM.

To examine the dependence of our results on domain size, as well as the fundamental role that the LW CRE plays in GCMs we run the fully parameterized experiments (P25 and P100) on a "small" and "large" domain. The long dimension of the small domains is 4,000 km and the long dimension of the large domain is 16,000 km. To explore the mock-Walker circulation in the context of both a GCM and a CRM we utilize comparisons of the experiments with grid-spacings of 100 km (P100), 25 km (P25 and E25), 2 km (E2), and 1 km (E1) all on a domain with the same long dimension of 4,000 km. The experiments with a grid-spacing of 25 km (P25 and E25) serve as a link between the GCM-like configuration and the CRM-like configuration. The only difference between these two experiments is that E25 has both the shallow and deep convective parameterizations turned off so that all of the convection in that experiment is explicit, as it is in E2 and E1. Domains with dimensions of 16,000 km were judged too costly for the 1 and 2 km experiments.

The E1 and E2 simulations are in many ways similar to the configuration of so-called cloud resolving models. In particular, all convection is explicitly resolved, and the threshold of grid-cell mean relative humidity which triggers new clouds is changed to 1.0 from the default value of 0.8. While a grid spacing of 1 or 2 km is clearly not small enough to resolve all clouds, it is small enough to resolve many clouds and cloud-systems. The large-scale cloud scheme is based on the Tiedtke (1993) parameterization. This was originally designed to be used with GCMs having a coarse grid-spacing and includes prognostic equations for both cloud liquid water and cloud fraction. However, we are not aware of a fundamental problem in using the Tiedtke scheme for large-scale clouds in a model with 1 km grid-spacing. The advantage of using the Tiedtke scheme is retaining the identical cloud scheme as is used in the parent GCM; the disadvantage is the greatly increased complexity of the cloud computations relative to many other cloud resolving models.

3. Cloud Radiative Interactions and the Organization of a Mock-Walker Circulation

3.1. General Characteristics of the Mock-Walker Circulation

The mock-Walker Circulation that emerges from these simulations is shown in Figures 1 and 2 to be characterized by a strong overturning circulation with precipitation focused over the warmer SSTs and a humid boundary layer across the full length of the domain. Superposing the circulation and relative humidity (Figure 1) clearly shows the result of subsidence driven drying over regions with cooler SST (at the edges of the domain) and the tropospheric moistening from ascending parcels which originate in the boundary layer over the region of high SST (in the center of the domain). To illustrate some of the sensitivities to convective parameterization and the interaction between clouds, radiation, and the large-scale circulation we compare the P25 experiment with analogous experiments in which the longwave CRE is turned off (P25 LWCRE-off, middle panels of Figure 1) and in which the convection is made explicit by turning off the convective parameterization (E25, right panels of Figure 1). The circulation is illustrated by the combination of the mass stream function in Figure 1 and the vertical velocity in Figure 2. The lower panels of Figure 1 show high concentrations of condensate in the mid-troposphere over the warmer SSTs, while the regions with subsiding circulations are dry ($RH < 20\%$) above about 900 hPa. Two distinct circulation cells are present with one below, and one above 500 hPa. This state of deep overturning circulation with convection and precipitation concentrated in the region of ascent and a dry troposphere in the regions of descent is common to the Walker circulation, tropical two-box models (e.g., Bretherton et al., 2006; Larson et al., 1999; Pierrehumbert, 1995), and experiments of radiative convective equilibrium which equilibrate to a state with deep-overturning circulations and convective aggregation (e.g., Bretherton et al., 2005).

When the coupling between the circulation and clouds is broken by making the clouds invisible to the LW radiation, the atmospheric state is more symmetric about the maximum SST and the weaker circulation is more spread out horizontally. The default configuration in which the clouds interact with the LW radiation
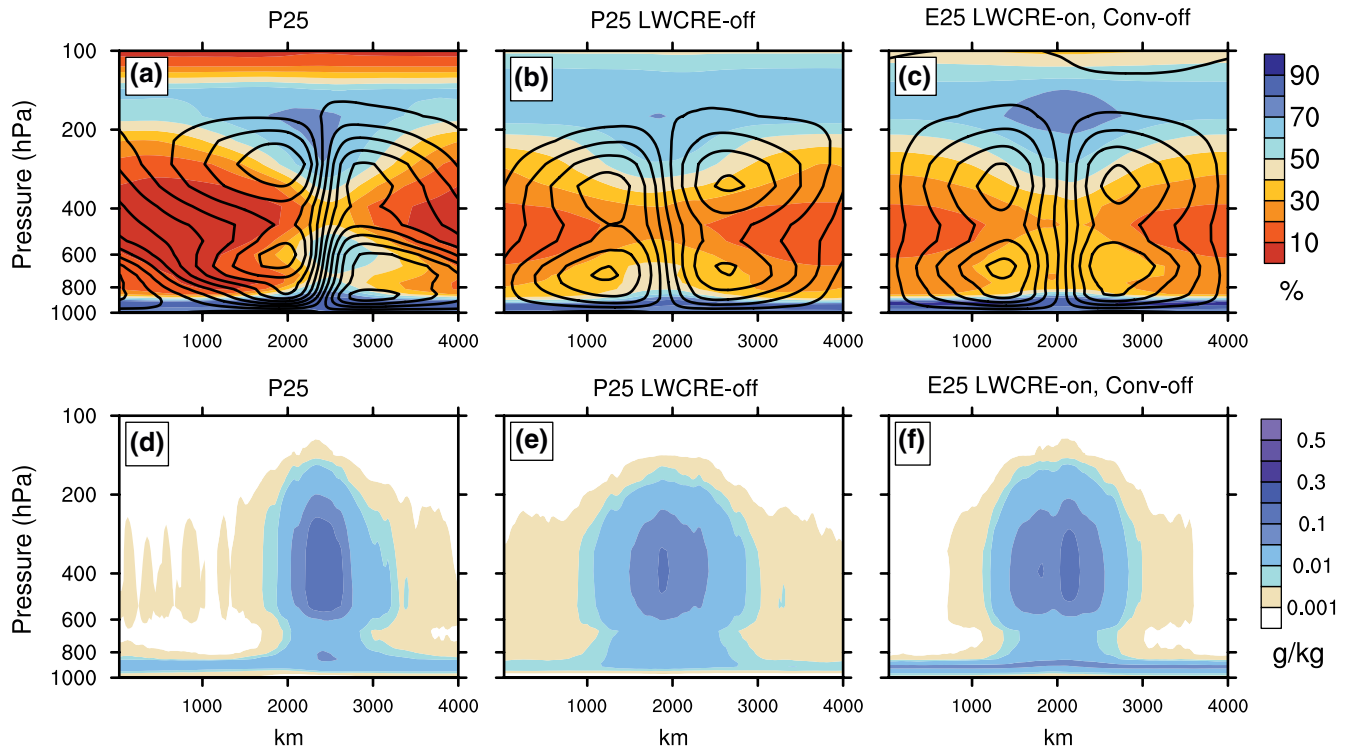
Figure 1. The equilibrated state of the Walker cell for three configurations with a grid-spacing of 25 km on a domain of $200 \times 4{,}000$ km^2. Top panels show relative humidity (shading) and mass stream function (black contours). The contour interval for the mass stream function is 6×10^9 kg/s. Lower panels show total (liquid + ice) condensate (g/kg). Deep and shallow convection are fully parameterized (P25) in panels (a) and (d), panels (b), and (e) show P25 LWCRE-off, and the experiment with LWCRE on, but the convective parameterization turned off (E25) is shown in panels (c) and (f).

results in a stronger, spatially concentrated circulation and will be discussed further in later sections (also seen Figures 4, 5, 9, and 10). Active LWCRE leads to lower values of domain mean OLR and higher domain mean precipitable water (PW) in all cases (Table 2).

Interactions between clouds and radiation play a dominant role in determining the fundamental characteristics of our system. The domain mean precipitation ($\overline{P}$) provides one example of this. Because of the energetic constraints that connect $\overline{P}$, atmospheric condensational heating, and the total radiative cooling, the time evolution of the precipitation is a useful measure of whether a model has reached a state of stationarity, or statistical balance. Figure 3 demonstrates that this balance is reached after about 30 days for the E2, and E1 simulations, and after roughly 100 days for the P25 and P100 simulations. Although the variability of $\overline{P}$ is fairly large (1–2 mm/d), after the initial adjustment period of a few months, the experiments are steady in time. This is demonstrated in Figure 3 with the colored circles and diamonds which show the mean values of $\overline{P}$ over the last 4 years (5 months) of the experiments for the GCM-like (CRM-like) experiments. After the initial adjustments the simulations all oscillate about mean precipitation values which tend to increase with the grid-spacing (Table 2). Despite the same boundary conditions and base model, these experiments have a large range of domain mean precipitation (Table 2) that varies by as much as 0.6 mm/d (3.5–4.1 in parameterized experiments; 3.1–3.7 in explicit experiments). Note that the GCM-like experiments have a larger $\overline{P}$ than the CRM-like experiments, and that the LWCRE leads to larger $\overline{P}$ in the GCM-like experiments but smaller $\overline{P}$ in the CRM-like experiments. This will be discussed further in Section 5. The large oscillations in $\overline{P}$ shown in Figure 3 are similar to those noted in previous studies (Patrizio & Randall, 2019; Silvers et al., 2016). Differences in $\overline{P}$ can be understood as a consequence of the differences in upper level cloud fraction and the surface energy budget and will be discussed further in Section 5.

One of the simplest measures of convective aggregation and the large-scale circulation is the subsidence fraction (SF), the fraction of the domain in which the mid-tropospheric air is subsiding (Coppin & Bony, 2015). As convection becomes more organized, or aggregated, the SF will increase. For an overturning circulation
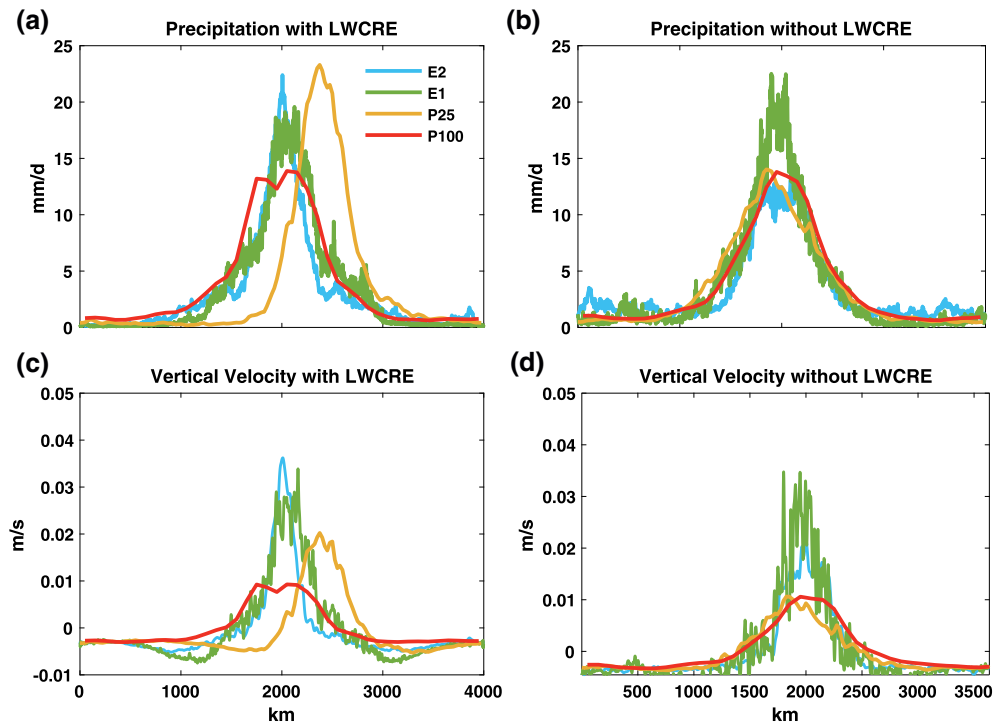
Figure 2. Precipitation (a) and (b) and vertical velocity (c) and (d) at approximately 530 hPa for P100, P25, E2, and E1 experiments. The data have been averaged over the short horizontal dimension of the channel and over the equilibrated part of the experiments. Panels (a) and (c) show the control configurations with default model physics. Panels (b) and (d) show the corresponding experiments with the longwave cloud radiative effect turned off (LWCRE-off).

a contraction of the convective region should result in a larger subsidence fraction. This is precisely what we see in Table 2. For each of our experiments with LWCRE-on the SF is larger than or equal to the case with LWCRE-off. The SF was calculated with the monthly mean pressure velocity on the 500 hPa pressure level averaged over the equilibrated period (last 4 years (months) for the GCMs (CRMs)). All of our experiments have an SF ≥ 0.72. This indicates that while our mock-Walker circulation is distinct from RCE and the resulting spontaneous self-aggregation, our region of persistent deep convection clearly corresponds to a state of aggregation. Using a mock-Walker circulation allows one to study controlled convective aggregation
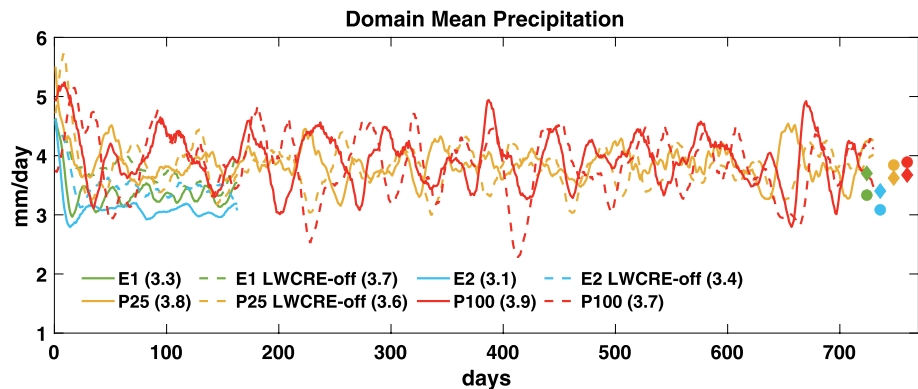

Figure 3. Domain mean precipitation as a function of time. Solid lines are the control experiments, dashed lines show the LWCRE-off experiments. All data is shown for the E1 and E2 experiments while for P25 and P100 only the first 2 out of 5 years is shown. The dots (control) and diamonds (LWCRE-off) at far right show the time mean values of precipitation for the last 4 years (P25, P100) and last 5 months (E1, E2). The mean values are also given in the legend. All data have been smoothed twice with a 9-days running mean filter.
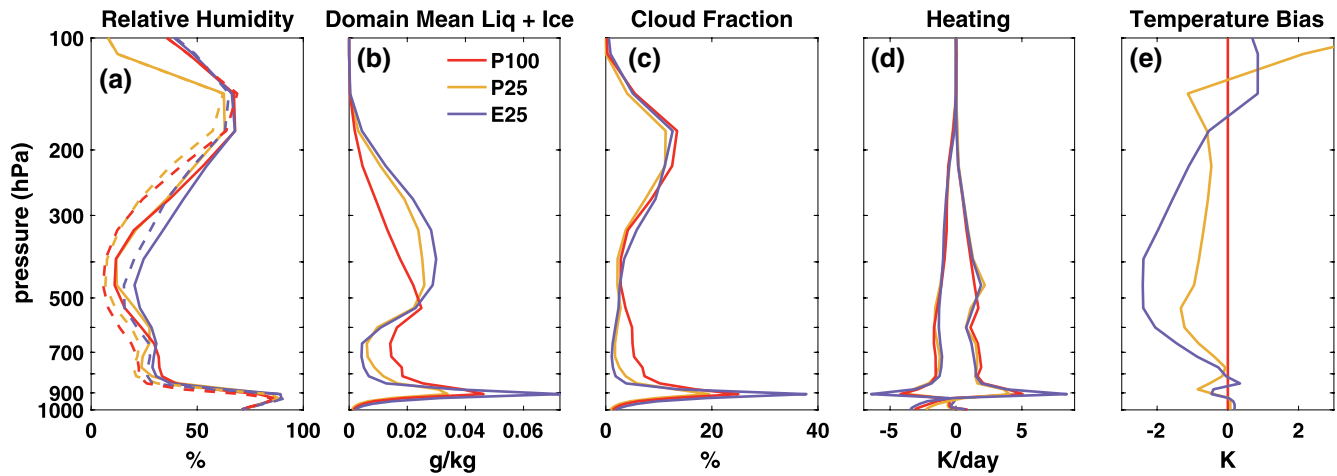
Figure 4. Domain mean vertical structure of the P100, P25, and E25 experiments. The dashed lines of relative humidity (a) show the values in the region with subsidence. The positive heating profiles (d) show the heating due to both convection and the large-scale cloud scheme, the negative profiles show the sum of the heating due to longwave and shortwave radiation. Panel (e) shows the atmospheric temperature relative to the P100 experiment.

rather then spontaneous convective self-aggregation. Previous studies have shown a dependence of aggregation on temperature (Cronin & Wing, 2017; Khairoutdinov & Emanuel, 2010; Wing & Emanuel, 2014), Table 2 illustrates how much the aggregated state can vary among experiments with identical SST. Having a
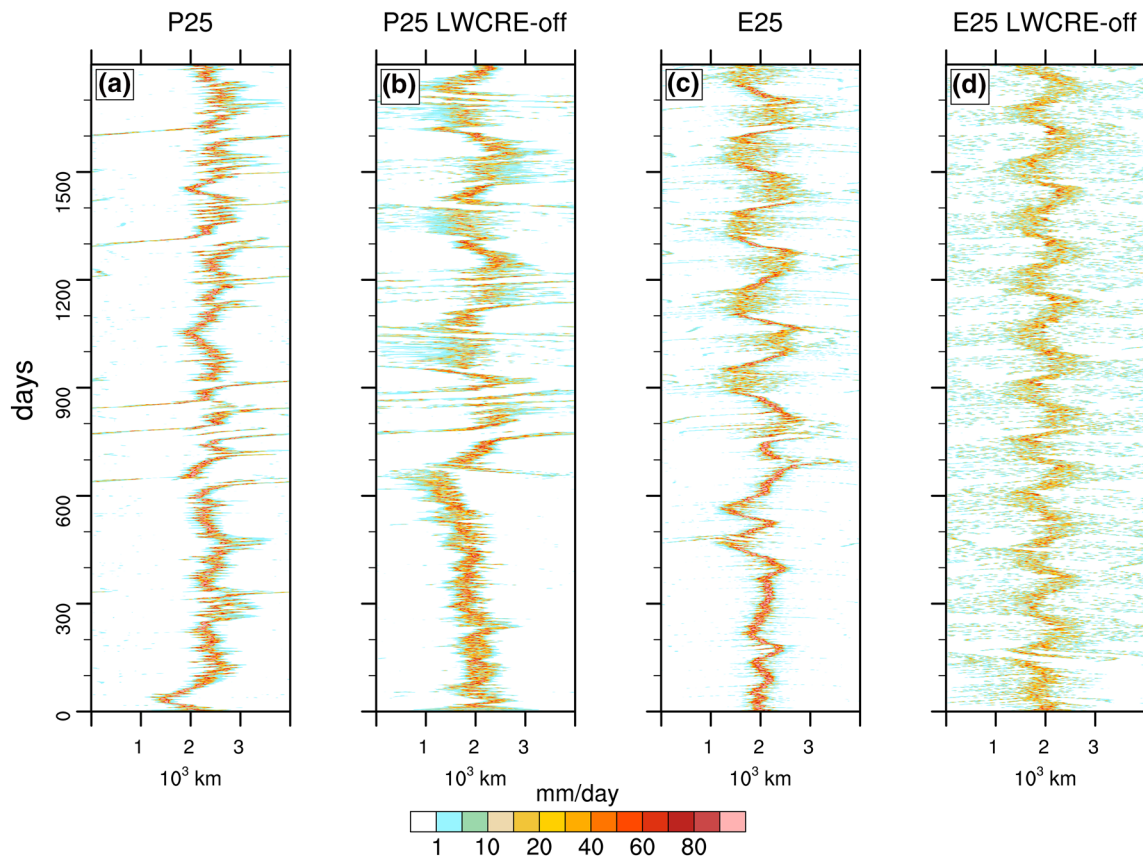

Figure 5. Evolution of precipitation through five years of simulation for four experiments with a grid spacing of 25 km. (a) Control 25 km experiment (P25); (b) P25 with LWCRE turned off; (c) Both deep and shallow convective parameterization schemes are turned off (E25); (d) E25 experiment shown in (c) except with the LWCRE turned off. All cases have an SST of 301 K at the center and 297 K at the edges. Contour values are: 1, 5, 10, 15, 20, 30, 40, 50, 60, 70, 80, and 90. Data have been averaged over the short horizontal dimension of the domain.
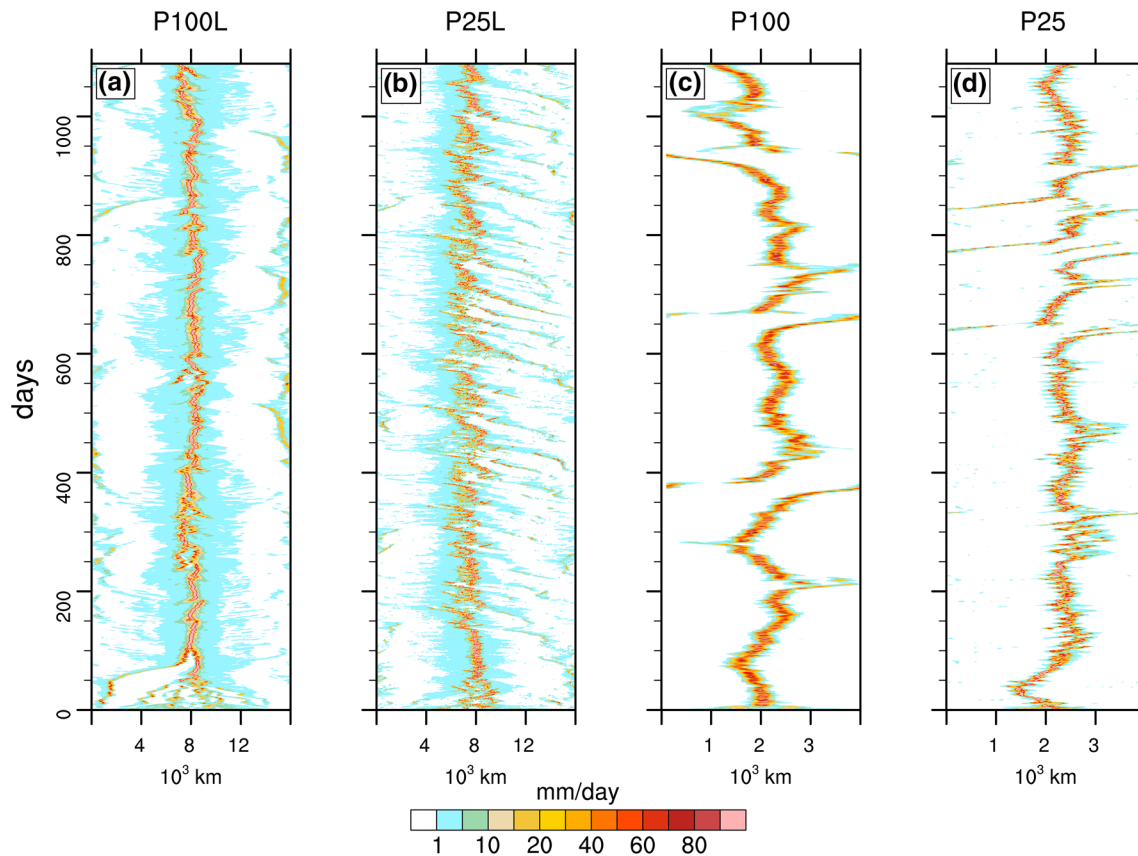
Figure 6. Evolution of precipitation through the first 3 years of simulation for experiments with a grid spacing of 25 and 100 km. (a) 100 km experiment on the large domain (P100 L); (b) 25 km on large domain (P25 L); (c) 100 km on small domain (P100); (d) 25 km on small domain (P25). For each resolution, the only difference between the experiments shown is a long edge length of 16,000 or 4,000 km. All cases have an SST of 301 K at the center and 297 K at the edges. Contour values are: 1, 5, 10, 15, 20, 30, 40, 50, 60, 70, 80, and 90. Data have been averaged over the short horizontal dimension.

prescribed SST warm patch ensures that the simulations will be "aggregated" to some degree. Given identical SSTs, the range of different SFs provide a measure of variability that is driven entirely by the interactions between convection, radiation, and the large-scale circulation.

3.2. Comparison of Experiments with Parameterized or Explicit Convection

Before analyzing the CRM-like experiments E1 and E2 in which there is no parameterized convection we examine the influence of the double plume convective parameterization in the P25 and P100 experiments and compare to the E25 experiment. The E25 experiment, identical to P25 except with fully explicit convection, then can serve as a link between the GCM-like experiments and the CRM-like experiments.

The mass stream function and vertical velocity both show the P25 (Figures 1a and 1d and 2) experiment to have a stronger, more concentrated overturning circulation than either the P25 LWCRE-off (Figures 1b and 1e) or E25 (Figures 1c and 1f) experiments. The control GCM-like experiment (P25) also has larger values of RH and more condensate in the convective region and a dryer subsidence region, relative to the P25 LWCRE-off and E25 experiments. Averaged over the full domain, the P25 case with parameterized convection results in a dryer atmosphere with

Table 2

Domain Mean Precipitation ($\overline{P}$), Outgoing Longwave Radiation ($\overline{OLR}$), Precipitable Water ($\overline{PW}$), and Subsidence Fraction (SF), the fraction of the domain that is subsiding at the 500 hPa level

Name	$\overline{P}\,(\mathrm{mm\,d^{-1}})$	$\overline{OLR}\,(\mathrm{W\,m^{-2}})$	$\overline{PW}\,(\mathrm{mm})$	SF
P100 L	4.1 (3.5)	283.1 (286.9)	36.6 (31.3)	0.82 (0.72)
P100	3.9 (3.7)	283.2 (296.4)	28.0 (26.8)	0.74 (0.74)
P25 L	4.0 (3.8)	281.2 (290.7)	35.0 (32.9)	0.81 (0.78)
P25	3.8 (3.7)	282.9 (293.6)	27.4 (26.4)	0.82 (0.80)
E25	3.7 (3.5)	271.9 (286.8)	28.7 (27.3)	0.82 (0.81)
E2	3.1 (3.4)	266.2 (285.5)	27.0 (25.2)	0.86 (0.81)
E1	3.3 (3.7)	269.3 (289.2)	27.3 (26.5)	0.82 (0.79)

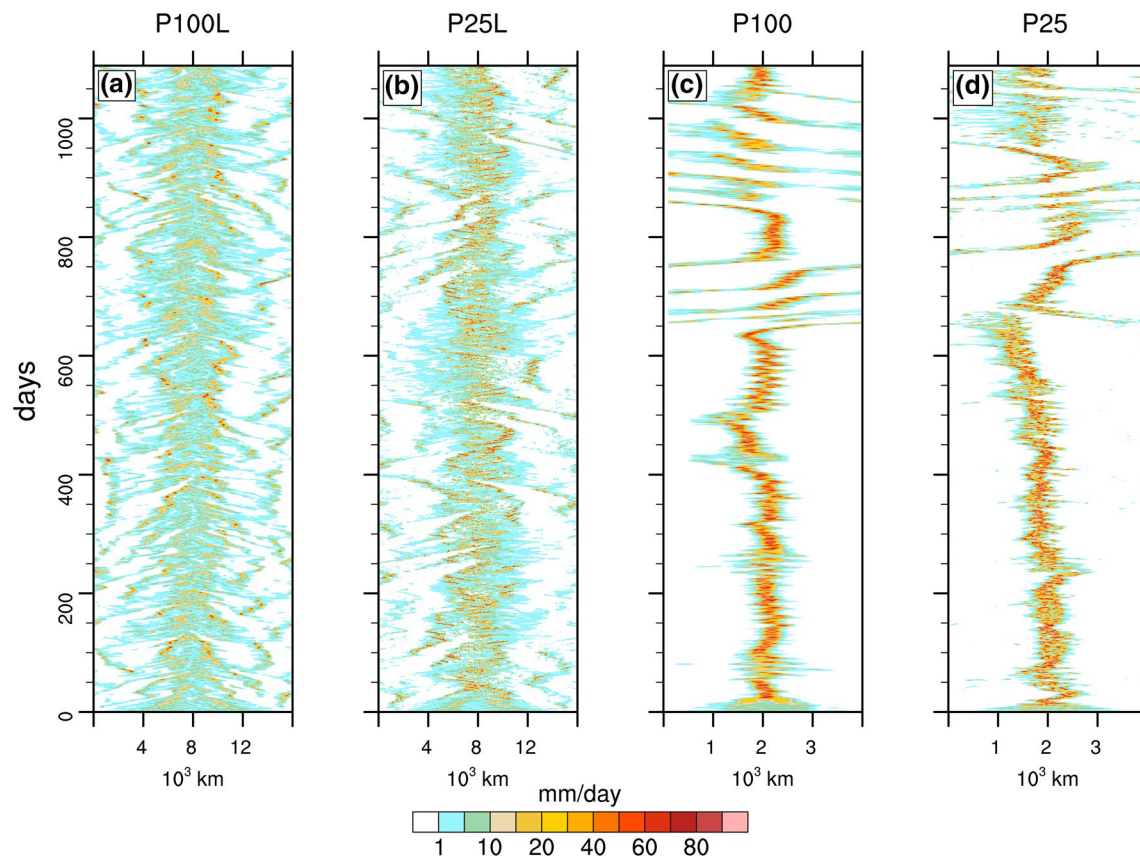*Note.* Values in parenthesis correspond to LWCRE-off experiments.

Figure 7. Identical to Figure 6, except that the clouds do not interact with the longwave radiation; the LWCRE is off.

less condensate (Figures 4a and 4b). Mean relative humidity profiles from the regions with mid-tropospheric subsidence (Figure 4a, dashed lines) further accentuate the dryness of P100 and P25 relative to E25.

The influence of different grid-spacing, and convective parameterization can be seen in the vertical profiles of several key variables for the P100, P25, and E25 experiments (Figure 4). Overall the experiments with parameterized convection transport more moisture (both condensate and water vapor) out of the boundary layer and into the lower troposphere. The parameterized experiments are also substantially warmer in the mid-troposphere compared to the E25 experiment which is forced to transport all moisture and heat with explicit dynamical motions. Near 900 hPa, relative to P25 and P100, the E25 experiment has nearly twice as much low-level condensate (Figure 4b), a cloud fraction that is, about 10% higher, larger condensational heating, and stronger cloud-top radiative cooling. It is also worth noting that for both P25 and P100, the condensational heating above 850 hPa (Figure 4d) is dominated by the large-scale cloud scheme rather than the convective parameterization. This is presumably because of the large-scale overturning circulation that is being forced by the SST pattern. Overturning circulations tend to trigger the large-scale cloud scheme. The fraction of precipitation that is due to either the large-scale or convective parameterizations will be discussed in the next section.

Figure 1 suggests that the strong asymmetries of the circulation, moisture fields, and precipitation in P25 could be eliminated by either turning off the convective paremeterization (E25) or by turning off the LW-CRE. Examining the evolving structure of the precipitation (Hovmöller diagrams) over the full 5 year simulations for P25, P25 LWCRE-off, E25, and E25 LWCRE-off offers additional insight into the role of the convective parameterization and the CRE. While the P25 experiment shows a fairly consistent irregularity (Figure 5a), both the P25 LWCRE-off (Figure 5b) and the E25 experiments (Figure 5c) have distinct patterns that can remain steady for years before changing. In contrast, the E25 LWCRE-off experiment (Figure 5d) shows a regular, zipper-like structure of strong precipitation that persists throughout the entire 5 years of the experiment.
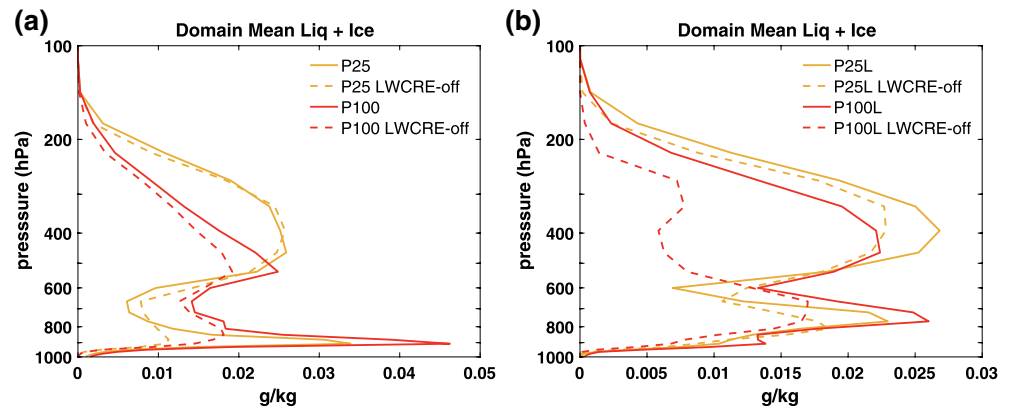
Figure 8. Domain mean total condensate (liquid + ice; grams/kilogram) on the domain with a long dimension of 4,000 km (a) and 16,000 km (b). P25 experiments are shown with yellow lines and P100 experiments with red. Solid lines show experiments with LWCRE on and dashed lines the LWCRE-off experiments.

One of the most prominent features of our GCM-like simulations is the erratic (relative to the symmetric SST distribution) structure of the precipitation field. This is particularly apparent in the P25 experiment on the small domain but is also present on larger domains and with a grid-spacing of 100 km (Figures 2, 6, and 9). The steady-state precipitation maximum is not consistently located over the warmest SST but is frequently shifted to slightly cooler temperatures. This signature is present in the vertical velocity, mass circulation, relative humidity, specific humidity, and radiative heating. In the Hovmöller diagrams (Figures 5–7), the precipitation appears to be averse to residing over the SST maximum. For the P25 case shown in Figure 1, a strong ($1 \, \text{m s}^{-1}$) domain mean shear develops above about 500 m which shifts the precipitation and circulation off center for years at a time. The P25 LWCRE-off experiment shows a symmetric circulation and condensate field, as well as a precipitation structure that is centered on the SST maximum for about four or five hundred days. When the convective parameterization is turned off and the LWCRE is on, (Figure 5c, E25), the overturning circulation becomes weaker and broader (seen in vertical velocity, and the mass stream function, Figures 1 and 2), and the precipitation, cloud fields, and circulation reside over the SST maximum for about 1 year. These experiments appear to be equilibrated after the first few months. It is therefore surprising to see in Figure 5 that after more than a year of simulation both the P25 LWCRE-off and the E25 experiments have dramatic changes in the time evolution of their precipitation ($\overline{P}$ does not change, Figure 3). The irregular precipitation patterns of our parameterized experiment result from the interactions between the convective parameterization scheme and the LWCRE. The experiments with convective parameterization (P25,P100) result in a dryer and warmer mid-troposphere and allow strong precipitation to occur even over the coldest SSTs.

4. The Influence of Domain Size on Low-Level Clouds and the Large-Scale Precipitation

The evolution in time of the precipitation field illustrates how much the spatial distribution can vary as a function of domain size, parameterization of convection, and the effect of the LW radiation due to clouds. Shown in Figures 6 and 7 are Hovmöller plots of precipitation after averaging along the short horizontal dimension. The four panels show simulations with two grid-spacings (25 km and 100 km) using two different domain sizes (long edge length of 4,000 km and 16,000 km). Figure 6 shows the control GCM-like experiments and Figure 7 shows the equivalent simulations with LWCRE-off. Previous studies of RCE (Bretherton et al., 2005, 2006; Dixit et al., 2018; Jeevanjee & Romps, 2013; Muller & Held, 2012; Patrizio & Randall, 2019; Silvers et al., 2016) have documented sensitivities of the equilibrated state to domain size. We have in most cases chosen to keep the long edge length fixed at 4,000 km. The analysis of the previous, and of the next section focuses on results from experiments using a domain with a long edge length of 4,000 km. However, when comparing those results to experiments with a long edge length of 16,000 km, we find interesting sensitivities to the domain size that are described in this section.
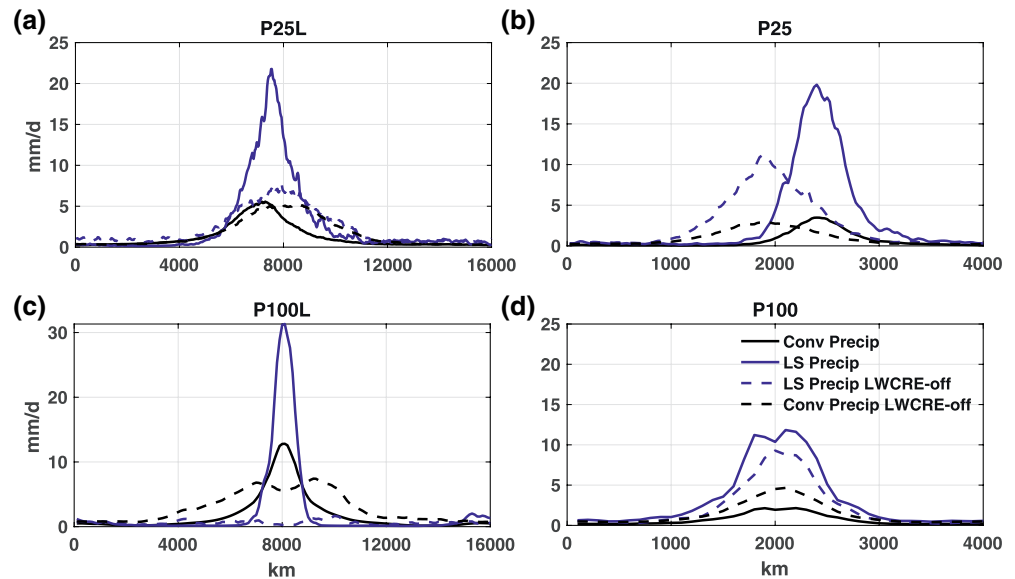
Figure 9. Precipitation due to the large-scale (blue) cloud scheme and the convective parameterization (black). Panels (a) and (c) show large domains with a long edge of 16,000 km while (b) and (d) show domains with a long edge of 4,000 km. LWCRE-off experiments are shown with dashed lines.

At all resolutions the Hovmöller plots show that the LWCRE acts to concentrate the precipitation over a smaller geographic extent. The structure of the precipitation changes more as a function of domain size than it does as a function of resolution. On the large domains, the difference between experiments with and without LWCRE is extreme (compare Figures 6a and 6b to 7a and 7b). In contrast to the control experiments in Figure 6 which all show a narrow region of strong precipitation meandering within about 500 km of the SST maximum at the center of the domain, the large domain experiments without the LWCRE have an 8,000 km wide region in which the precipitation consistently develops (Figure 7). Smaller cells and lines of precipitation develop within this large area with no apparent preference to settle over the center of the domain where the SST is a maximum. There is also a dramatic change in the distribution of precipitation on the 4,000 km domain simulations after almost 2 years. The domain mean precipitation does not significantly change in these cases, only the spatial structure.

An additional unexpected change that results from increasing the domain size is an upward shift of the cloud fields. The low-level condensate has a cloud base that decreases in magnitude and shifts from near 900 hPa in the small domain (thin lines, Figure 8) to between 700 and 800 hPa in the large domain (thick lines) simulations. There is also a vertical shift in the upper-level ice condensate, but it is less pronounced. As the domain size increases, so too does the domain mean precipitable water ($\overline{PW}$) which varies by as much as 30% among the experiments (Table 2). Smaller domains (1,024 km compared to 4,096 km wide) were found to have a more focused ascent region, larger precipitation rates, and less low-level clouds in the CRM simulations of Bretherton et al. (2006). In contrast, here smaller domains have more low-level clouds and slightly less precipitation rates (Table 2, Figure 8).

The domain mean total precipitation is constrained by the radiative cooling of the atmosphere. However, in models with the convection parameterized, the total precipitation is composed of precipitation from the convection scheme and the large-scale cloud scheme. The relative contribution of each component is not well constrained and Held et al. (2007) have shown that the fraction of the precipitation that is due to the large-scale cloud scheme is closely linked to low-cloud cover and total condensate. The distribution of convective and large-scale precipitation indicates how the condensational heating in a GCM is being distributed among the parameterizations, and what is triggering the precipitation. Precipitation from each of these two components is shown in Figure 9 as a function of resolution and domain size. In the regions of large-scale ascent, most of the precipitation derives from the large-scale cloud scheme. Following the terminology of Held et al. (2007) we could say that most of the precipitation is coming from gridpoint storms in which
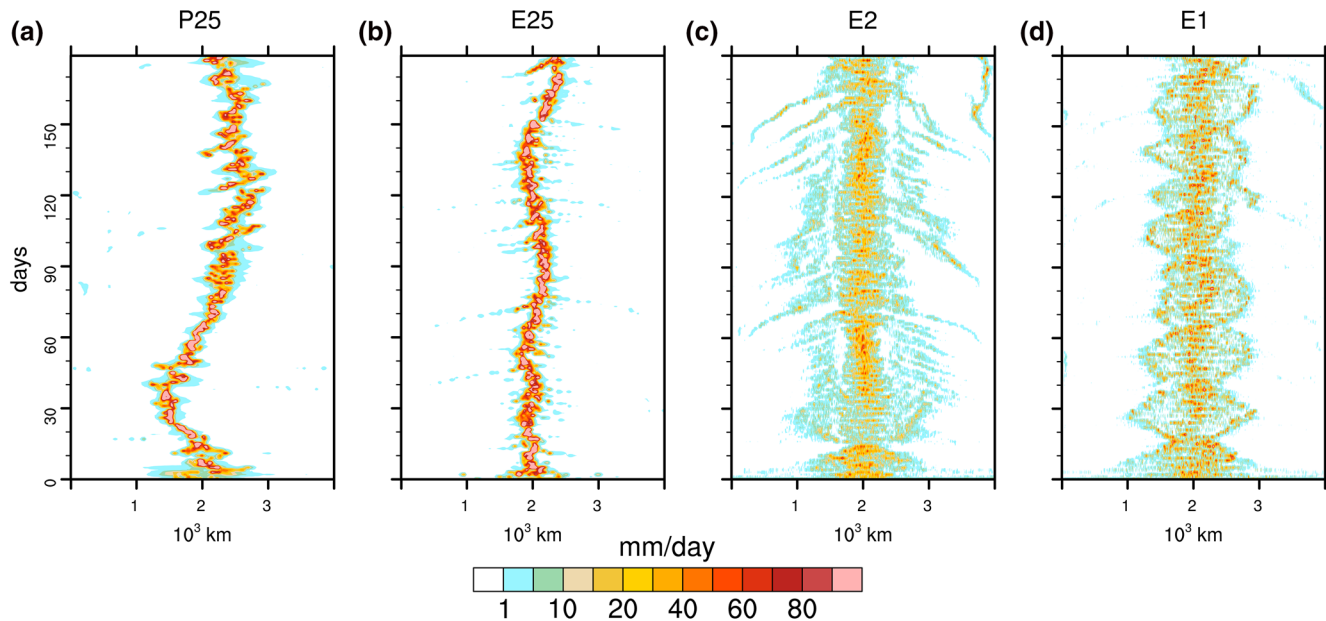
Figure 10. Evolution of precipitation through the first 6 months of simulation for (a) the 25 km control case (P25), (b) 25 km case with no parameterized convection (E25), (c) 2 km control (E2), and (d) 1 km control (E1). All panels have a long edge width of 4,000 km with the center of the domain having a prescribed SST of 301 K and the edges 297 K. Data have been averaged over the short horizontal dimension.

the upper level moisture is being supplied not by the convective parameterization but from the boundary layer as a result of large-scale upwelling. We also see that the LWCRE (solid lines) dramatically increases the large-scale precipitation. The LWCRE has a much smaller effect on the magnitude of the convective precipitation but does act to spatially concentrate it. With the exception of the P100 L LWCRE-off experiment, the convective precipitation produces relatively little of the total precipitation. Figure 9 shows that the dramatic dependence on domain size of the precipitation field that is seen in Figure 7 corresponds to a decrease in the large-scale precipitation of about 65% in the P25 L case and an almost complete elimination of the large-scale precipitation in the P100 L case for the LWCRE-off case. We do not find a dependence on grid-spacing of the large-scale or convective precipitation. The fraction of precipitation that is due to the large-scale cloud scheme was linked to the low-level cloud radiative effect in Held et al. (2007).

The fact that the partitioning of precipitation by the convective and large-scale parameterizations depends on both the size of the domain and the LW CRE could imply that the changes of the low-level clouds are being influenced by sensitivities within the parameterized physics which influence the partitioning of precipitation.

5. From a General Circulation to Cloud Resolving Model: Dependence on Resolution

We now use the mock-Walker circulation to compare GCM-like simulations to CRM-like simulations. This section focuses on simulations with grid-spacing of 1, 2, and 25 km all on a domain with the width of 4,000 km for the long edge. The models agree on the basic circulation pattern and the spatial distribution of mid-tropospheric condensate. However, the E25/P25 simulations produce 4–5 times as much low-level cloud and condensate as E2/E1 in the subsiding regions. As a result, the models have a different response to the LWCRE. In the atmospheric boundary layer, the differences among the models of the wind, enthalpy flux, and temperature result in different spatial distributions and amounts of precipitation in the equilibrated state.

Notable differences in the structure of the precipitation that result from the overturning circulation at different resolutions are shown in Figure 10. Shown are 180 days of precipitation from the P25 (left to right), E25, E2, and E1 simulations. As the resolution increases the distribution of precipitation becomes broader,
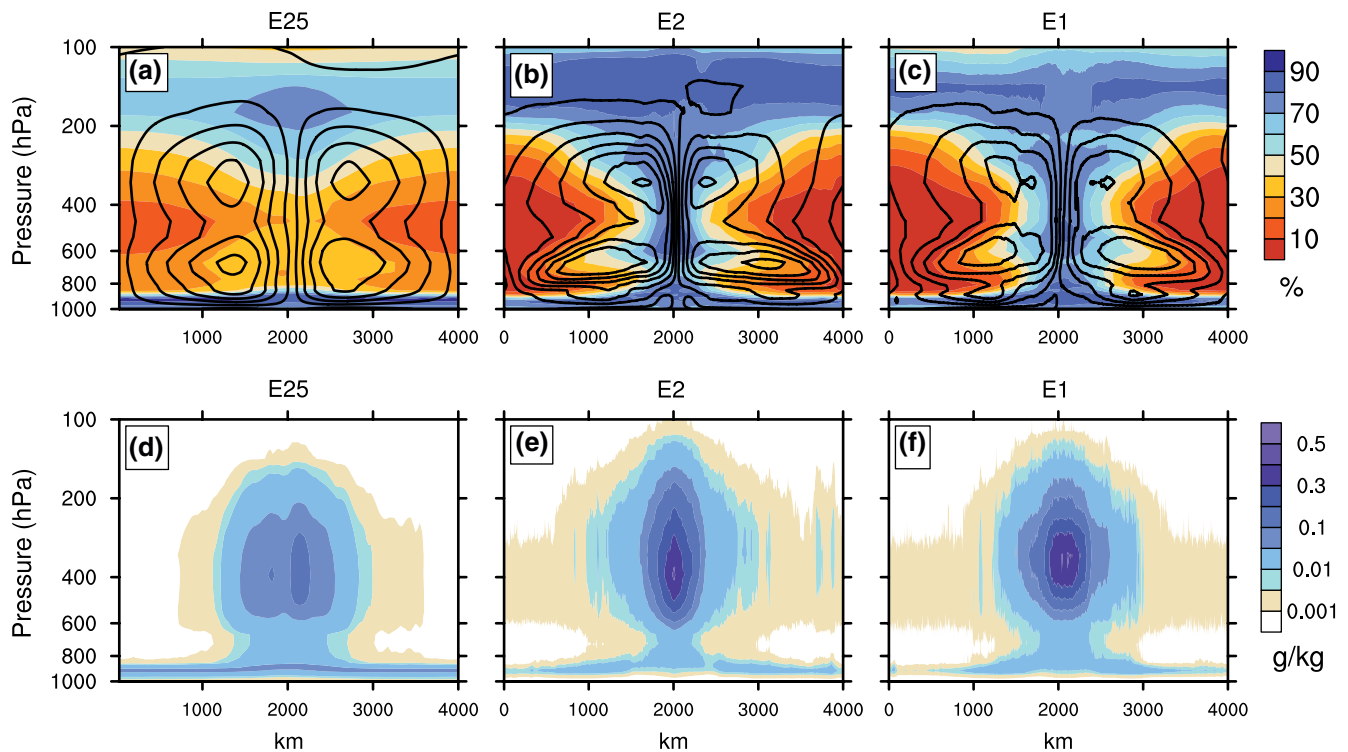
Figure 11. The equilibrated state of the Walker cell as a function of resolution. (a) and (d) show E25, (b) and (e) show E2, and (c) and (f) show E1. Top panels show the steady state relative humidity (shading) and mass stream function (black contours) while bottom panels show the total condensation (liquid + ice). Contour interval for the mass stream function is 6×10^9 kg/s.

more consistently centered over the SST maxima, and has lower maximum precipitation rates. Note that both the P25 and E25 simulations show more variability at later times compared to these first 180 days (see Figures 5a and 5c). The simulations with explicit convection at resolutions typical of cloud-resolving models (E2, E1) show little aversion to the precipitation maximum occurring over the maximum in SST. Relative to the P100, P25, and E25 simulations, the cloud resolving simulations are able to maintain a smoother distribution of precipitation over a broader range of SST values. Complex patterns of precipitation over a fixed sinusoidal or Gaussian SST distribution have been noted many times in previous literature (Bretherton et al., 2006; Grabowski et al., 2000; Jeevanjee et al., 2017; Wofsy & Kuang, 2012). The irregularities have tended to be symmetric about the SST maximum. This is broadly consistent with our simulations when the convection is entirely explicit (E25, E2, and E1), but is strikingly different than for the P25 and P100 experiments.

The influence of resolution on the atmospheric state can be clearly seen in the two-dimensional structure of circulation and humidity (Figures 11 and 12). Perhaps the most obvious similarity is the double celled structure in the mass stream function and the most obvious difference being the humidity in the center of the domains where the RH differs by as much as 40%. All experiments show a mid-tropospheric relative humidity minimum over the cooler SSTs where subsidence dominates. The E25 experiment has a fairly symmetric double celled structure in stark contrast to the irregular circulation that is, present in the P25 experiment (Figure 1). A small third cell has developed in the boundary layer of the 1 km experiment. The high resolution experiments also have higher amounts of condensate throughout the troposphere, and much higher relative humidity above 200 hPa.

Compared to E25, the E1 and E2 experiments have stronger deep overturning circulations and substantially more condensate aloft above the warm patch. It is also apparent in Figures 11 and 12 that the condensate below 800 hPa decreases with increasing resolution. This is consistent with an overturning circulation that strengthens as the resolution increases and transports more moisture from the low-levels to the mid-troposphere. It is also consistent with weaker mixing from shallow clouds with decreased resolution as discussed
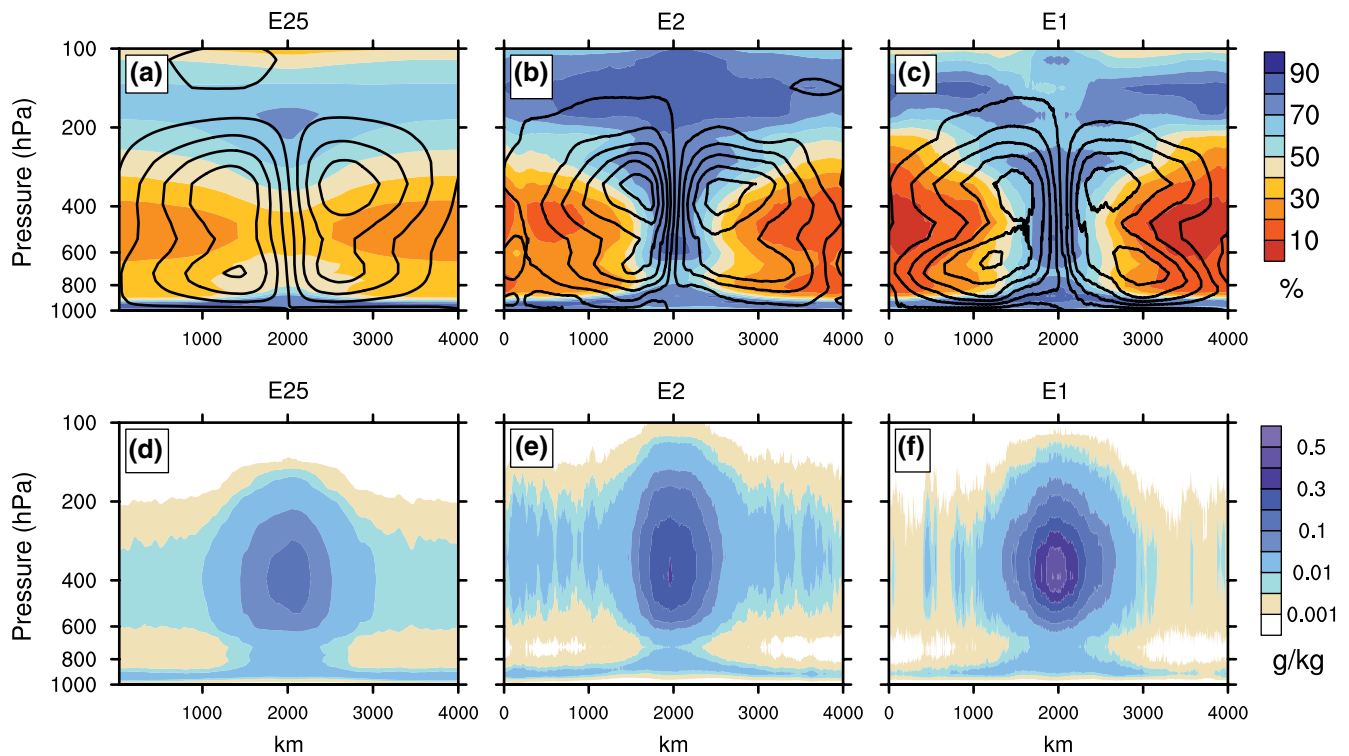
Figure 12. Same as previous figure except with the longwave CRE turned off.

in Pauluis and Garner (2006). Figure 12, with LWCRE-off, shows greater asymmetries and generally weaker circulations below about 500 hPa. When the clouds and radiation directly interact with each other the experiments have a more organized and stronger circulation below 500 hPa. Figures 11 and 12 also show that the E2 and E1 simulations are more similar when the clouds and radiation interact than they are with LWCRE-off. The subsidence region drying and condensate aloft in the upwelling region have a clearer dependence on resolution for the LWCRE-off experiments. This suggests that the interactions between
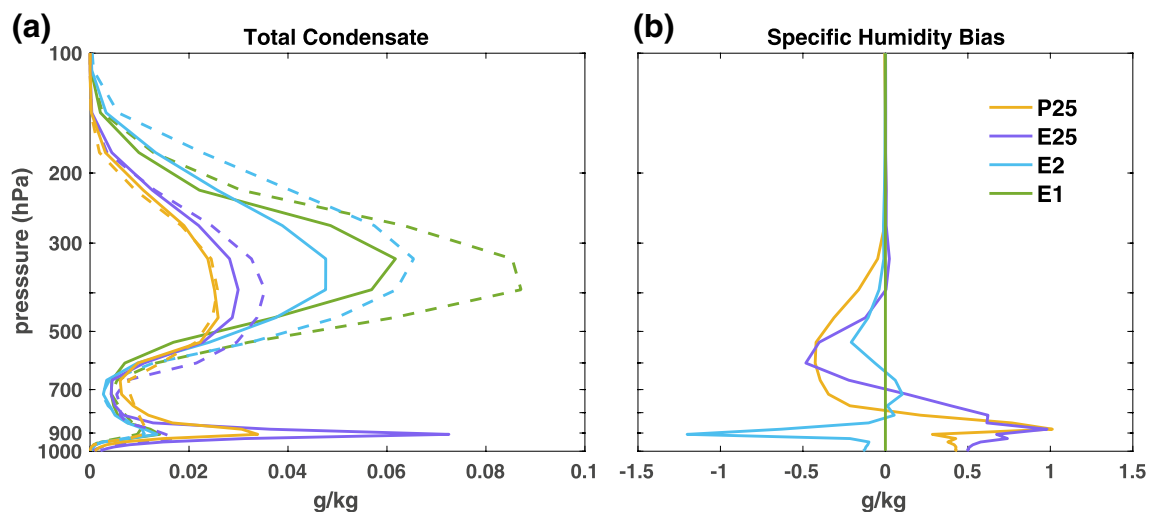

Figure 13. Domain mean profiles of water species. (a) Total condensate (liquid + ice), liquid condensate is less than 0.005 g/kg above 600 hPa, and (b) specific humidity bias, computed relative to E1. Solid lines show LWCRE on experiments and dashed lines show the LWCRE-off experiments.
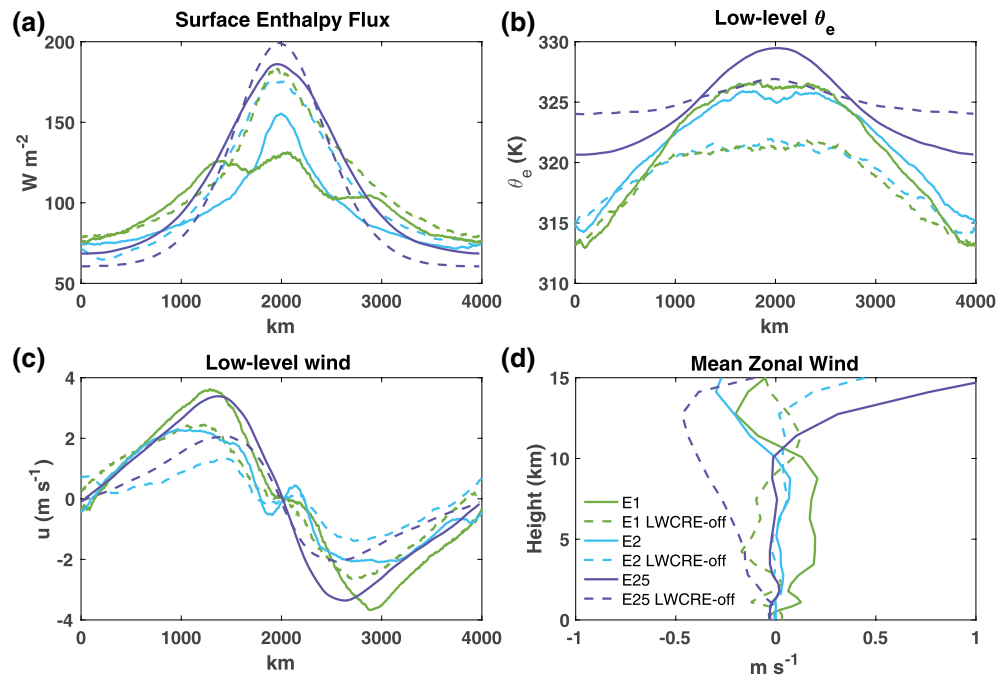
Figure 14. Low-level structure and domain mean wind shear for simulations with explicit convection. The surface enthalpy flux (a) is the latent plus sensible heat flux. Also shown are the equivalent potential temperature (b) and zonal wind (c) at the lowest model level in the atmosphere. Panel (d) shows the domain mean zonal wind profiles.

clouds and radiation help the atmosphere to converge toward a particular state that is less dependent on resolution.

The domain mean condensate is closely related to the distribution of clouds and the flow of energy through the atmosphere. The condensate and the specific humidity provide clues about the strength of convection and the vertical mass transport. Figure 13a shows the domain mean condensate for P25, E25, E2, and E1 (solid lines) and the corresponding experiments with the LWCRE-off (dashed lines). Figure 13b shows the vertical distribution of specific humidity relative to the E1 experiment. Profiles similar to Figure 13a but for the experiments with parameterized convection were discussed in the previous section (Figure 8). The GCM-like P100, P25, and E25 experiments have much higher values of low-level liquid condensate while the CRM-like E2 and E1 experiments have much higher values of upper-level ice condensate. Below about 800 hPa, Figure 13b shows more moisture for the E25 and P25 experiments, relative to the E1 and E2 experiments. Above about 800 hPa E25 and P25 have less moisture. The profiles in Figures 13a and 13b combined with the stronger circulations over the SST maximum for the E1 and E2 experiments all imply that the dynamics of the E1 and E2 experiments are transporting enough condensate and specific humidity aloft to dry out the 200 hPa nearest to the surface relative to the E25 and P25 experiments. This results in far fewer low-level clouds for the E1 and E2 experiments and could also explain the high values of ice in those experiments. Although our experiments differ from RCE, the results are consistent with Pauluis and Garner (2006) who showed that for decreasing resolution an RCE model had a moist bias in the sub-cloud layer and a dry bias in the troposphere above.

The LWCRE plays a major role in determining the equilibrium RH, total condensate, and LW radiative heating of the troposphere. This is highlighted by comparing experiments with and without the LWCRE. The upper panels of Figures 11 and 12 show that the interactions between LW radiation and clouds lead to an enhanced drying of the troposphere in regions of subsidence (relative to LWCRE-off). This is especially true for the E1 and E2 simulations. Interactive LWCRE leads to less upper level ice-condensate for our CRM-like experiments with the effect increasing as the resolution increases (Figure 13). The opposite occurs with GCM-like experiments (Figure 8) for which interactive LWCRE increase the amount of upper level ice-condensate. Below about 700 hPa turning off the LWCRE leads to a strong
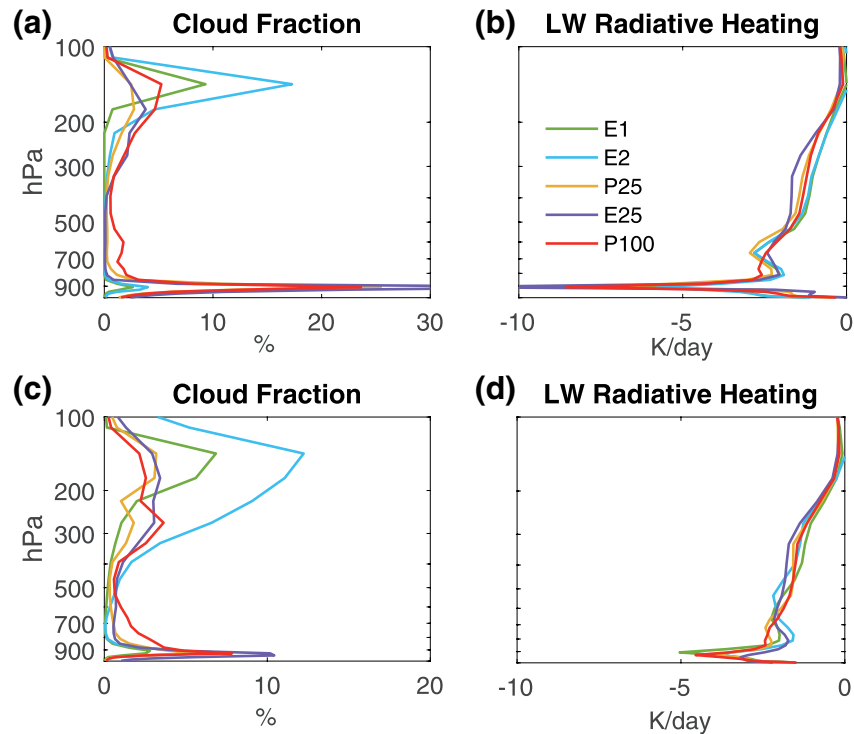
Figure 15. Cloud fraction and temperature tendency due to longwave radiation in subsidence regions. (a) and (b) show the control experiments while (c) and (d) show the analogous LWCRE-off experiments. Subsidence regions are defined as the quarter of the domain farthest from the SST maximum, that is, at the center of the domain. Note the change of axis between (a) and (c).

decrease in condensate in the GCM-like experiments, but a negligible decrease in the condensate of the CRM-like experiments. The profiles of diabatic cooling are similar among all LWCRE-off experiments (Figure 15). But when the LWCRE is on, the GCM-like experiments have up to twice as much diabatic cooling as the CRM-like experiments below 850 hPa. The manifestation of interactions between clouds and radiation as indicated by these characteristics differ dramatically between the GCM-like and CRM-like experiments.

Despite a fairly regular distribution of precipitation around the SST maximum for experiments with increasing resolution, the surface enthalpy flux (latent plus sensible heat fluxes) reveals large differences in the symmetry of the near surface energetics. Figure 14 shows the surface enthalpy flux, the equivalent potential temperature, and the u-component wind field for E1, E2, and E25. Over the SST maximum, E25 has a surface enthalpy flux that is, 60 W/m^2 larger than that of the E1 experiment, and the E1 experiment has an irregular pattern of enthalpy flux in the middle half of the domain. These differences in magnitude and regularity are apparently due to differences in the low-level wind speeds among the experiments. For the LWCRE-off experiments, the difference in the enthalpy flux between E25 and E2/E1 over the warmest SSTs is reduced from 60 W/m^2 to about 20 W/m^2 and the enthalpy flux for E1 and E2 are very similar. Thus even for the case of prescribed SSTs and no land surface the interactions between clouds and the LW radiation have a massive influence on the surface energy budget.

It is also interesting to note that despite stronger low-level winds, E25, E2, and E1 all have a weaker surface enthalpy flux when the clouds and radiation are allowed to interact. As represented by bulk parameterizations, both the sensible heat flux and the latent heat flux are directly proportional to the magnitude of a measure of the low-level wind. However, the sensible and latent heat fluxes are also proportional to the gradient of moisture and temperature between the surface and lowest atmospheric level. E25, E2, and E1 all show an increased amount of specific humidity (not shown) in the lowest atmospheric model level that is reflected in the equivalent potential temperature (Figure 14b). This

implies that the vertical gradient of moisture and temperature is smaller when the LWCRE is active and thus accounts for the lower surface enthalpy flux relative to the LWCRE-off experiments. It is also worth noting that in contrast to the P25 case which has strong domain mean shear, E25 has less domain mean wind shear then E1.

We now turn our attention to the clouds in the regions of subsidence over the cooler SSTs. Figure 15a shows E2 to have the largest (about 17%) upper-level mean cloud fraction in the subsidence region, with the E1 experiment having the next largest cloud fraction (10%), followed by P100, E25, and P25 (3%−5%). As noted in the discussion of the total condensate, the CRM-like models produce large values of upper-level cloud with minimal low-level clouds while the GCM-like models do the opposite with large amounts of low-level clouds and 5% or less of upper level-couds. Figures 15b and 15d shows that the differences among the upper-level clouds only slightly shifts the radiative cooling in the upper troposphere, but the differences in low-level clouds correspond to a strong change of the radiative cooling around 900 hPa.

An interesting point that emerges from the domain mean values of precipitation ($\overline{P}$, see Table 2) is that the sign of the response to LWCRE is not the same between CRM and GCM experiments. When clouds are not allowed to interact with the LW radiation, the atmosphere emits more radiation to space, as evidenced by larger values of $\overline{OLR}$ for all LWCRE-off experiments. Net atmospheric radiative cooling can be thought of as a proxy for the mean precipitation because the cooling is usually balanced primarily by condensational heating. All else remaining equal, larger values of $\overline{OLR}$ would then correspond to larger values of $\overline{P}$. This is clearly not the case for the E25, P25, and P100 experiments. The domain mean precipitation rates decrease despite an increased amount of $\overline{OLR}$. The implication is that the requisite atmospheric heating must come from a process other than condensation.

Examining the energy budget of the surface and the role played by the low-level clouds reveals the source of the extra atmospheric heating for the E25, P25, and P100 experiments. Prescribed SST generates a constant upward flux of LW radiation. The upward flux of sensible heat flux will be mostly fixed (barring variations in surface wind) because changes in the downward flux of solar radiation will not warm the surface. Low-level clouds, especially in dry regions, serve as a significant source of radiative cooling for the atmosphere (Figure 15) because they increase the downwelling longwave radiation. Making these clouds invisible to radiation creates a source of effective atmospheric warming by removing a source of atmospheric energy loss. Invisible low-level clouds also allow the upwelling LW flux of radiation to play a larger role in warming the atmosphere. These two factors more than compensate for the increased OLR at the Top of the Atmosphere of the LWCRE-off experiments. There is an increase in atmospheric warming on the order of 20 W m^{-2} for the LWCRE-off experiments and thus additional condensational heating is not needed to balance the increase of OLR. Thus $\overline{P}$ actually decreases (Table 2). These results for E25, P25, and P100 are consistent with Popp and Silvers (2017) who showed less condensate in the atmosphere and much less precipitation (at the equator) for LWCRE-off experiments (see their Figure 1). The large decrease of low-level clouds when the LWCRE is off also leads to an increase of downward shortwave radiation at the surface. Because of the low albedo of water this only slightly increases the fluxes of reflected shortwave radiation (about 2 W m^{-2}) and contributes minimally to heating the atmosphere. With an interactive surface, the surface temperature would be influenced by the downward flux of both LW and shortwave radiation that a change of cloud fraction would lead to.

In contrast to the E25, P25, and P100 experiments just discussed, E1 and E2 have larger $\overline{P}$ for the LWCRE-off experiments. This can be explained as follows. One of the primary methods by which the LWCRE influences the atmosphere is by heating the atmosphere in the region between the clouds and the surface. Larger values of ice condensate and upper-level cloud fraction as seen in the E2 and E1 experiment (Figure 13) therefore imply a larger atmospheric heating due to the CRE relative to the E25, P25, and P100 experiments in which there are fewer clouds aloft (Figures 8, 13, and 15). When the warming effect of the upper level clouds in the E1 and E2 experiments is removed in the LWCRE-off experiments the energy balance of the atmosphere is maintained through an increase of latent heating and subsequent increase of precipitation (Table 2).
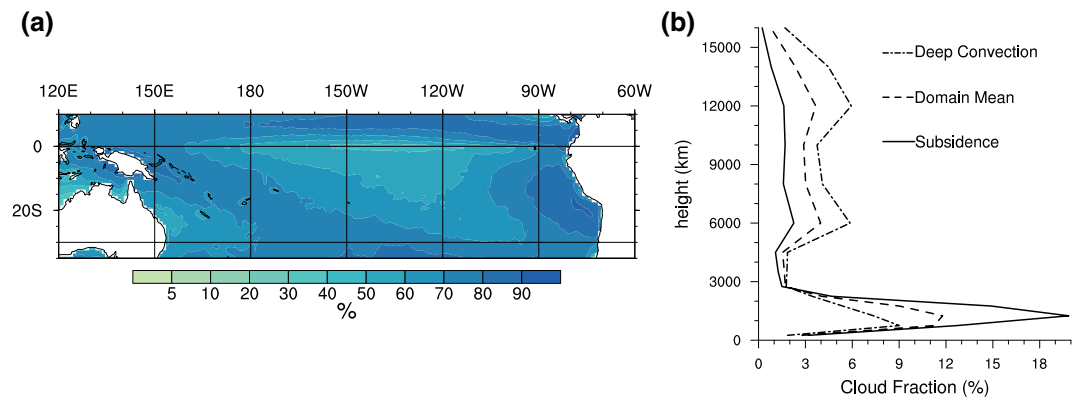
Figure 16. Observations of cloud fraction in the tropical Pacific from the Satellite-based MISR data over the years 2000–2019. (a) Time averaged cloud fraction in the tropical Pacific region. (b) Cloud fraction as a function of height from the region of (a) dominated by subsidence (solid), the mean of the full domain (long dashes) shown in (a), and the mean from a region of (a) characterized by frequent deep convection (dash-dot), see text for details. The latitudinal extent plotted in (a) follows that used by Schwendike et al. (2014) in their description of the regional Walker circulation (see their Figure 2).

These experiments provide insight into the different mechanisms by which the clouds in GCMs and CRMs interact with LW radiation in the atmosphere. Because there are so many more low-level clouds in the GCM-like experiments there is a strong response to upwelling radiation from the surface. In contrast, in the CRM-like experiments the abundance of upper-level ice condensate, and lack of low-level condensate, results in the primary interaction between clouds and radiation being in the atmosphere below the upper-level clouds.

In order to make a qualitative connection to observed clouds and hopefully motivate a more detailed comparative study Figure 16 shows the clouds observed with the Multiangle Imaging Spectro-Radiometer (MISR) instrument on board NASA's Terra satellite (see Marchand et al. [2010] for details). We use the domain (10N-35S) which was identified by Schwendike et al. (2014) as the geographic region corresponding to the regional Walker circulation in the Pacific. Figure 16a shows the cloud fraction averaged from March 2000–November 2019 of the full domain of the Pacific regional Walker circulation. This region includes much of the so-called warm pool beneath the ascending branch of the Walker Circulation as well as the eastern Pacific subsidence regions that encompass the stratocumulus cloud decks that are common off the west coast of South America. Figure 16b shows three profiles of cloud fraction from this region. These profiles are calculated by summing the MISR data across all optical depths over the domain mean (dashed line), a region of subsidence (10° N–35°S; 120°–60°W, solid line), and a region that is, characterized by deep convection (10°N–35°S; 120°E–180°, dash-dot line). Overall, both the upper-level (2%) and low-level (20%) cloud fraction from the subsiding region of MISR are closer to the cloud profiles simulated by the GCM-like models (Figure 15a, E25, P25, and P100). The CRM-like simulations are more realistic in the sense that they resolve much more of the turbulent dynamic motions that influence cloud systems. But the low level clouds that dominate the regions of the Walker circulation under subsiding motion depend on sub-kilometer scale resolutions and must be parameterized using the large-scale cloud scheme. We expect that the difference between our GCM-like and CRM-like responses to the LW radiation would be minimized if the large-scale cloud scheme was tuned in the CRM-like experiments to produce low-level cloud fractions that better matched observations. Our results indicate that at the CRM-like resolutions we investigate the details of the large-scale cloud scheme are a key element in the realism of the simulation. It should be kept in mind that there are several substantial differences between our mock Walker circulation and the observed Walker circulation.

6. Conclusions and Discussion

In this section, we conclude by summarizing the primary results of our study, followed by a brief discussion of the context and implications of these results.

6.1. Summary of Results

We have used the framework of the tropical overturning circulation, specifically the Walker Circulation, to compare the multi-scale interactions between large-scale circulations, cloud systems, and interactive radiation across experiments with grid-spacing ranging from 1 to 100 km. To better isolate the role that clouds and humidity play in driving and responding to the circulation, experiments have been performed with and without the radiative effect of clouds, with and without the convective parameterization, and with multiple domain sizes. Our results show that the convective parameterization and the longwave cloud radiative effect (LWCRE) strongly interact with each other and often lead to precipitation structures that do not settle over the SST maxima, as well as large differences in the equilibrated atmospheric state.

Perhaps the most interesting result is that the GCM-like experiments have a relatively large low-level cloud fraction while the CRM-like experiments have a large upper-level cloud fraction. This difference in the dominant cloud type leads to opposite atmospheric responses to changes of the LWCRE. The LWCRE increases the domain mean precipitation ($\overline{P}$) for the GCMs but decreases it for the CRMs (Table 2). Over the regions with cooler SSTs, the large low-level cloud fraction of the GCMs acts as a source of radiative cooling that is balanced by condensational heating in the control case. A strong decrease of low-level clouds in the GCMs for the LWCRE-off experiments removes this cooling and condensational heating. The increase of precipitation that is expected in the LWCRE-off case as a result of increased LW cooling to space is not enough to overcome the effective heating that results from the decrease of clouds at low-levels, with a net effect of less $\overline{P}$. Over the regions with cooler SSTs, the CRMs have very few (less than 5%) low-level clouds and as a result the change of $\overline{P}$ is driven by the increased LW cooling to space in the LWCRE-off case. Watanabe et al. (2018) found a similar relationship between low-clouds and precipitation in the context of climate change experiments. This highlights how sensitive the energetics of the tropical atmosphere are to the distribution of clouds and their interaction with the radiation.

Decreasing the grid-spacing from 100 to 1 km allowed for the parameterization of both deep and shallow convection to be turned off, resulting in a more direct simulation of the dynamics that are fundamental to the overturning tropical circulation. Relative to simulations with a grid-spacing of 100 and 25 km, the 1 and 2 km experiments have the following characteristics:

- Overturning circulations are stronger and more consistently centered over the maximum of SST (Figure 2)
- Between 300 and 800 hPa in the upwelling regions the E1 and E2 models have a relative humidity as much as 50% larger than the lower resolution simulations (Figures 1 and 11)
- Above about 600 hPa, there is two to four times more ice condensate, but less than half as much liquid condensate below 700 hPa (Figure 13)
- The E1 and E2 experiments have about 10%–25% less $\overline{P}$ (3.1–3.7 mm/d) compared to P25 and P100 (3.5–4.1 mm/d). See Table 2

Three striking changes occur as a result of a four-fold increase in domain width. The low-level clouds shift upward by more than 100 hPa (Figure 8), there is a dramatic widening of the precipitation distribution in the LWCRE-off experiments (compare Figures 6 and 7), and the LWCRE mediates the precipitation from the large-scale cloud parameterization but not the convective precipitation (Figure 9). This impact on the large-scale precipitation occurs for the GCM-like experiments on smaller domains as well, but is pronounced in the large domain experiments. This dependence on domain size could imply that 4,000 km is not large enough to contain the largest scales that are important for the overturning circulation. Another reason for the domain size dependence could be the changing scale of the warm and cold regions of SST.

It is remarkable that despite having the same prescribed SST and incoming radiation the control simulations (LWCRE on) have a precipitation rate that can vary by as much as 25%, wildly different precipitation structures, and surface enthalpy fluxes that vary by as much as 60 W/m^2 (Table 2, Figures 6, 10, and 14). All simulations use the same dynamical core, radiation, turbulence, large-scale cloud, and microphysics parameterizations. Results from these experiments demonstrate that the cloud type plays a fundamental role in determining how the radiative fluxes couple the large-scale circulation to the moisture. The large differences in the surface

enthalpy flux appear to be due to differences in the winds near the surface (Figure 14). The large influence of the low-level wind and enthalpy flux on the structure of precipitation, low-level moisture and clouds, and mid-tropospheric humidity in the convective regions is consistent with previous studies showing the importance of the low-level wind fields for precipitation (Fermepin & Bony, 2014; Wofsy & Kuang, 2012), boundary layer properties (Raymond, 1994), and even the climate sensitivity (Silvers et al., 2016).

Our results show a stronger overturning circulation (Figures 1, 2, and 11) in the CRM-like experiments compared to the GCM-like experiments. Accompanying this is a difference in the vertical mixing of water condensate, specific humidity and temperature (Figures 4, 8, and 13). We conclude that the CRM-like experiments (E1 and E2) transport more specific humidity and liquid water from the lowest 200 hPa of the atmosphere into the troposphere above than do the GCM-like experiments (P100 and P25). While the E25 experiment does not use convective parameterizations, in terms of the vertical distribution of water species and clouds it is more similar to the GCM-like experiments than to the CRM-like experiments.

7. Discussion

Many of the previous studies of mock-Walker circulations or simplified models of tropical dynamics (e.g., Bretherton & Sobel, 2002; Larson et al., 1999; Neelin & Zeng, 2000; Peters & Bretherton, 2005; Pierrehumbert, 1995; Raymond, 1994; Sobel et al., 2004) have focused on simplifying the physics parameterizations as much as possible while still maintaining the interactions between convection and radiation. These have proven useful but have remained complex enough to make comparisons with other models difficult, and the degree to which the simplifying assumptions influence the conclusions is unclear. The approach of this paper is different. We study an idealized configuration with the full complexity of a GCM. Pierrehumbert (1995) argued that cloud processes are not the leading cause of the stable tropical climate but that it is, "the ability of the atmospheric circulation to create dry air pools in regions of large-scale subsidence" – these are the "Radiator Fins" – , that serve as a cooling (thus stabilizing) mechanism for Earth's tropical climate. Our results demonstrate how strongly the cloud radiative effects influence the circulations that set up the Radiator Fins. Experiments with prescribed SST preclude the possibility of studying feedbacks between the circulation, and the relative area of warm and cold SST regions as Pierrehumbert (1995) did. However, our study shows how the interactions between clouds, radiation, and the circulation lead to changes in the area of the dry regions above the boundary layer. These dry regions allow the tropics to efficiently cool to space and maintain an energetic balance.

Using mock-Walker simulations to benchmark a GCM with a CRM was proposed by Jeevanjee et al. (2017). This was part of our initial motivation but is predicated on physics parameterizations that are simple enough to allow for a clean comparison. Utilizing something like Kessler microphysics, fixed radiative cooling, and a binary large-scale cloud scheme would provide an elegant comparison between models. However, making such changes to the GCM used in this paper would result in a model so different from AM4.0 that the CRM would no longer serve as a benchmark for AM4.0. We have chosen to keep the GCM as close as possible to AM4.0. More intermediate steps are necessary to create a clean link between CRMs and GCMs.

Our results also show that the mock-Walker circulation is an ideal configuration with which to test developments in large-scale cloud or microphysics parameterization schemes. This is an important step in the ongoing process of merging GCMs and CRMs into a global CRM.

There is a rich literature on tropical overturning circulations. While this study has interpreted the experiments in the context of the Walker Circulation, our results are also relevant to the overturning circulations and meridional SST gradients that define the Intertropical Convergence Zone (ITCZ) and the Hadley Circulation. In that context, our results are consistent with those of several recent studies (e.g., Albern et al., 2018; Dixit et al., 2018; Fermepin & Bony, 2014; Fläschner et al., 2018; Harrop & Hartmann, 2016; Popp & Silvers, 2017). Those studies, as well as the present one, show that the LWCRE acts to constrain, or tighten, the deep convective region. This results from an increased atmospheric energy uptake and strengthening of the overturning circulation where the deep convective clouds occur (Popp & Silvers, 2017). Also consistent with this previous work, the present paper shows that the LWCRE has a strong influence on the low-level circulation. When the LWCRE is turned off, the low-level circulations shift upward and are not as well organized

(Figures 11 and 12). There is a corresponding change in the low-level cloud fields, LW radiative cooling, and the domain mean precipitation. For the experiments with a GCM-like configuration, the LWCRE strongly influences the precipitation from the large-scale cloud scheme while leaving the precipitation from the convective parameterization scheme largely unchanged. This contributes to a much stronger response of the GCM-like experiments to the LWCRE, especially in the low-levels of the troposphere. Albern et al. (2018) showed that there is a large spread in the CRE response to warming among GCMs. Our expectation is that the fraction of precipitation that is due to the convective parameterization will be particular to individual GCMs. The disparate influence of the LWCRE on the large-scale precipitation could explain some of the model spread in the CRE response to warming.

The flexible modeling system at GFDL has allowed us to use a single code base in a GCM-like configuration with physics parameterizations that are very close to the AM4.0/CM4.0 models as well as in a CRM-like configuration with explicit convection. While there are significant differences between the CRM presented in this paper and more conventional CRMs (e.g., vertical grid spacing and a threshold based "binary" cloud scheme), the prospect of so easily converting a GCM into something like a CRM provides an enticing testbed for seeking process level understanding and future model development. This can be thought of as a top-down approach to developing a global CRM which should complement efforts that start with a regional large-eddy simulation (LES) model or CRM model and work toward a global model (e.g., Satoh et al., 2019; Schneider et al., 2017, 2019). The comparisons presented in this paper have highlighted some of the unexpected behaviors of a GCM-like configuration when used with idealized boundary conditions. Two examples include the consistently off-center circulations, and precipitation patterns, relative to the fixed SST pattern, and the dominance of the large-scale precipitation over the convective precipitation. The comparisons have also illustrated some of the challenges that arise when dramatically increasing the resolution of a GCM. These include the lack of shallow clouds in our CRM (both convective and stratocumulus) and the difficulty of comparing clouds in this CRM to other CRMs due to the prognostic large-scale cloud scheme. These are not fundamental challenges and motivate future work.

Mock-Walker cell configurations are an important step between models of RCE and models which simulate a wider range of Earth like conditions. The only difference between our simulations and RCE is the gradient of SST at the lower boundary. This simple difference from pure RCE creates a concrete link with the observed tropical atmosphere.

Studies using RCE have been fruitful but insufficient to fully illuminate the key processes behind the coupling of clouds, radiation, and the large-scale circulation, while typical GCM studies can be prohibitively complex. Many of the characteristics from RCE experiments with convective aggregation are present in mock-Walker simulations. For example, deep convection is anchored to a single location with high humidity and is surrounded by dry subsiding regions. It would be interesting to see how consistent the degree of aggregation and drying is among different models, as well as the response to warming SSTs. The configuration of a mock-Walker circulation is ideal for studying the effects of aggregation in a system that is more constrained than pure RCE. Prescribing a warm region of SST does not fully determine the large-scale circulation. This paper clearly shows how much variability there still is between the large-scale circulation, clouds, and fluxes of energy (radiative and surface enthalpy). The initial results from the RCE Model Intercomparison Project (RCEMIP; Wing et al., 2020) show a wide range of variability in the temperature, humidity, and clouds among the models. Adding the extra constraint of an overturning circulation forced by a prescribed gradient of SST, similar to the recent work of Shamekh et al. (2020) and Müller and Hohenegger (2020) would provide a context within which the wide range of results from RCEMIP could be reexamined and expanded upon.

Increasing computing resources will continue to blur the line that distinguishes GCMs from CRMs. As the grid-spacing of models decreases so too does the necessity of representing convection with parameterizations. As a result, the details of the large-scale cloud scheme will be increasingly important in the development of both GCMs and CRMs. For high resolution models with explicit convection, the upper-level clouds dominate the impact of interactions between clouds and radiation, but for GCM-like simulations the low-level clouds dominate this impact. Determining the respective roles of high and low clouds as medi-

ators between radiative effects and the large-scale overturning circulations in the observable atmosphere should be a high priority in future research.

Data Availability Statement

The code for the AM4.0 model is available for download at https://data1.gfdl.noaa.gov/nomads/forms/am4.0/, scripts used to perform the analysis and create figures are available on the GitHub repository https://github.com/gitleviglenn/SilversWalkerCell.git. Data used for analysis and to create figures in this manuscripts are available at ftp://nomads.gfdl.noaa.gov/users/Levi.Silvers/DoublyPeriodicWlkr/GFDL-AM4_doubly_periodic/and have the digital object identification of: https://doi.org/10.5281/zenodo.4047074. The MISR data were provided by Roger Marchand and is available at https://atmos.uw.edu/~roj/nobackup/MISR_observations/MISR_CTH_OD_histograms/, the original HDF MISR data is archived at the NASA Langely Atmospheric Science Data Center.

References

Albern, N., Voigt, A., Buehler, S. A., & Grützun, V. (2018). Robust and nonrobust impacts of atmospheric cloud-radiative interactions on the tropical circulation and its response to surface warming. *Geophysical Research Letters*, *45*(16), 8577–8585. https://doi.org/10.1029/2018GL079599

Andrews, T., & Webb, M. J. (2018). The dependence of global cloud and lapse rate feedbacks on the spatial structure of tropical pacific warming. *Journal of Climate*, *31*, 641–654. https://doi.org/10.1175/JCLI-D-17-0087

Bjerknes, J. (1969). Atmospheric teleconnections from the equatorial Pacific. *Monthly Weather Review*, *97*(3), 163–172.

Bretherton, C. S., Blossey, P. N., & Khairoutdinov, M. (2005). An energy-balance analysis of deep convective self-aggregation above uniform SST. *Journal of the Atmospheric Sciences*, *62*(12), 4273–4292. https://doi.org/10.1175/JAS3614.1

Bretherton, C. S., Blossey, P. N., & Peters, M. E. (2006). Interpretation of simple and cloud-resolving simulations of moist convection–radiation interaction with a mock-Walker circulation. *Theoretical and Computational Fluid Dynamics*, *20*(5), 421–442. https://doi.org/10.1007/s00162-006-0029-7

Bretherton, C. S., & Sobel, A. H. (2002). A simple model of a convectively coupled walker circulation using the weak temperature gradient approximation. *Journal of Climate*, *15*(20), 2907–2920. https://doi.org/10.1175/1520-0442(2002)015⟨2907:ASMOAC⟩2.0.CO;2

Coppin, D., & Bony, S. (2015). Physical mechanisms controlling the initiation of convective self-aggregation in a general circulation model. *Journal of Advances in Modeling Earth Systems*, *7*, 2060–2078. https://doi.org/10.1002/2015MS000571

Cronin, T. W., & Wing, A. A. (2017). Clouds, circulation, and climate sensitivity in a radiative-convective equilibrium channel model. *Journal of Advances in Modeling Earth Systems*, *9*(8), 2883–2905. https://doi.org/10.1002/2017MS001111

Dixit, V., Geoffroy, O., & Sherwood, S. C. (2018). Control of ITCZ width by low-level radiative heating from upper-level clouds in aquaplanet simulations. *Geophysical Research Letters*, *45*(11), 5788–5797. https://doi.org/10.1029/2018GL078292

Fermepin, S., & Bony, S. (2014). Influence of low-cloud radiative effects on tropical circulation and precipitation. *Journal of Advances in Modeling Earth Systems*, *6*(3), 513–526. https://doi.org/10.1002/2013MS000288

Fläschner, D., Mauritsen, T., Stevens, B., & Bony, S. (2018). The signature of shallow circulations, not cloud radiative effects, in the spatial distribution of tropical precipitation. *Journal of Climate*, *31*(23), 9489–9505.Retrieved from https://doi.org/10.1175/JCLI-D-18-0230.1

Fueglistaler, S. (2019). Observational evidence for two modes of coupling between sea surface temperatures, tropospheric temperature profile, and shortwave cloud radiative effect in the tropics. *Geophysical Research Letters*, *46*(16), 9890–9898. https://doi.org/10.1029/2019GL083990

Geisler, J. E. (1981). A linear model of the walker circulation. *Journal of the Atmospheric Sciences*, *38*(7), 1390–1400. https://doi.org/10.1175/1520-0469(1981)038⟨1390:ALMOTW⟩2.0.CO;2

Gill, A. E. (1980). Some simple solutions for heat-induced tropical circulation. *Quarterly Journal of the Royal Meteorological Society*, *106*(449), 447–462. https://doi.org/10.1002/qj.49710644905

Grabowski, W. W., Yano, J.-I., & Moncrieff, M. W. (2000). Cloud resolving modeling of tropical circulations driven by large-scale SST gradients. *Journal of the Atmospheric Sciences*, *57*(13), 2022–2040. https://doi.org/10.1175/1520-0469(2000)057⟨2022:CRMOTC⟩2.0.CO;2

Harris, L. M., & Lin, S.-J. (2013). A two-way nested global-regional dynamical core on the cubed-sphere grid. *Monthly Weather Review*, *141*(1), 283–306. https://doi.org/10.1175/MWR-D-11-00201.1

Harrop, B. E., & Hartmann, D. L. (2016). The role of cloud radiative heating within the atmosphere on the high cloud amount and top-of-atmosphere cloud radiative effect. *Journal of Advances in Modeling Earth Systems*, *8*(3), 1391–1410. https://doi.org/10.1002/2016MS000670

Held, I. M., Zhao, M., & Wyman, B. (2007). Dynamic radiative–convective equilibria using GCM column physics. *Journal of the Atmospheric Sciences*, *64*(1), 228–238. https://doi.org/10.1175/JAS3825.11

Iipponen, J., & Donner, L. (2020). Simple analytic solutions for a convectively driven walker circulation and their relevance to observations. *Journal of the Atmospheric Sciences, EOR*. https://doi.org/10.1175/JAS-D-20-0014.1

Jeevanjee, N., Hassanzadeh, P., Hill, S., & Sheshadri, A. (2017). A perspective on climate model hierarchies. *Journal of Advances in Modeling Earth Systems*, *9*(4), 1760–1771. https://doi.org/10.1002/2017MS001038

Jeevanjee, N., & Romps, D. M. (2013). Convective self-aggregation, cold pools, and domain size. *Geophysical Research Letters*, *40*(5), 994–998. https://doi.org/10.1002/grl.50204

Johnson, R. H., Rickenbach, T. M., Rutledge, S. A., Ciesielski, P. E., & Schubert, W. H. (1999). Trimodal characteristics of tropical convection. *Journal of Climate*, *12*(8), 2397–2418. https://doi.org/10.1175/1520-0442(1999)012⟨2397:TCOTC⟩2.0.CO;2

Khairoutdinov, M., & Emanuel, K. A. (2010). Aggregated convection and the regulation of tropical climate. *Proceedings of the 29th conference on hurricanes and tropical meteorology*. Boston, MA: American Meteorological Society.

Kuang, Z. (2012). Weakly forced mock Walker cells. *Journal of the Atmospheric Sciences*, *69*(9), 2759–2786. https://doi.org/10.1175/JAS-D-11-0307.1

Larson, K., Hartmann, D. L., & Klein, S. A. (1999). The role of clouds, water vapor, circulation, and boundary layer structure in the sensitivity of the tropical climate. *Journal of Climate*, *12*(8), 2359–2374. https://doi.org/10.1175/1520-0442(1999)012⟨2359:TROCWV⟩2.0.CO;2

Marchand, R., Ackerman, T., Smyth, M., & Rossow, W. B. (2010). A review of cloud top height and optical depth histograms from MISR, ISCCP, and MODIS. *Journal of Geophysical Research*, *115*(D16), 1–25. https://doi.org/10.1029/2009JD013422

Muller, C. J., & Held, I. M. (2012). Detailed investigation of the self-aggregation of convection in cloud-resolving simulations. *Journal of the Atmospheric Sciences*, *69*(8), 2551–2565. https://doi.org/10.1175/JAS-D-11-0257.1

Müller, S. K., & Hohenegger, C. (2020). Self-aggregation of convection in spatially varying sea surface temperatures. *Journal of Advances in Modeling Earth Systems*, *12*(1), e2019MS00169. https://doi.org/10.1029/2019MS001698

Neelin, J. D., & Zeng, N. (2000). A quasi-equilibrium tropical circulation model – Formulation. *Journal of the Atmospheric Sciences*, *57*(11), 1741–1766. https://doi.org/10.1175/1520-0469(2000)057⟨1741:AQETCM⟩2.0.CO;2

Patrizio, C. R., & Randall, D. A. (2019). Sensitivity of convective self-aggregation to domain size. *Journal of Advances in Modeling Earth Systems*, *11*(7), 1995–2019. https://doi.org/10.1029/2019MS001672

Pauluis, O., & Garner, S. (2006). Sensitivity of radiative–convective equilibrium simulations to horizontal resolution. *Journal of the Atmospheric Sciences*, *63*(7), 1910–1923. https://doi.org/10.1175/JAS3705.1

Peters, M. E., & Bretherton, C. S. (2005). A simplified model of the walker circulation with an interactive ocean mixed layer and cloud-radiative feedbacks. *Journal of Climate*, *18*(20), 4216–4234. https://doi.org/10.1175/JCLI3534.1

Pierrehumbert, R. T. (1995). Thermostats, radiator fins, and the local runaway greenhouse. *Journal of the Atmospheric Sciences*, *52*(10), 1784–1806. https://doi.org/10.1175/1520-0469(1995)052⟨1784:TRFATL⟩2.0.CO;2

Popp, M., & Silvers, L. G. (2017). Double and single ITCZs with and without clouds. *Journal of Climate*, *30*(22), 9147–9166. https://doi.org/10.1175/JCLI-D-17-0062.1

Radel, G., Mauritsen, T., Stevens, B., Dommenget, D., Matei, D., Bellomo, K., et al. (2016). Amplification of El Nino by cloud longwave coupling to atmospheric circulation. *Nature Geoscience*, *9*(2), 106–110. https://doi.org/10.1038/ngeo2630

Randall, D. A., Harshvardhan, Dazlich, D. A., & Corsetti, T. G. (1989). Interactions among radiation, convection, and large-scale dynamics in a general circulation model. *Journal of the Atmospheric Sciences*, *46*(13), 1943–1970. https://doi.org/10.1175/1520-0469(1989)046⟨1943:IARCAL⟩2.0.CO;2

Raymond, D. J. (1994). Convective processes and tropical atmospheric circulations. *Quarterly Journal of the Royal Meteorological Society*, *120*(520), 1431–1455. https://doi.org/10.1002/qj.49712052002

Satoh, M., Stevens, B., Judt, F., Khairoutdinov, M., Lin, S.-J., Putman, W. M., et al. (2019). Global cloud-resolving models. *Current Climate Change Reports*, *5*(3), 172–184. https://doi.org/10.1007/s40641-019-00131-0

Schneider, T., Kaul, C. M., & Pressel, K. G. (2019). Possible climate transitions from breakup of stratocumulus decks under greenhouse warming. *Nature Geoscience*, *12*(3), 163–167. https://doi.org/10.1038/s41561-019-0310-1

Schneider, T., Teixeira, J., Bretherton, C. S., Brient, F., Pressel, K. G., Schär, C., et al. (2017). Climate goals and computing the future of clouds. *Nature Climate Change*, *7*, 3–5. https://doi.org/10.1038/nclimate3190

Schwendike, J., Govekar, P., Reeder, M. J., Wardle, R., Berry, G. J., & Jakob, C. (2014). Local partitioning of the overturning circulation in the tropics and the connection to the Hadley and Walker circulations. *Journal of Geophysical Research: Atmospheres*, *119*(3), 1322–1339. https://doi.org/10.1002/2013JD020742

Shamekh, S., Muller, C., Duvel, J.-P., & D'Andrea, F. (2020). How do ocean warm anomalies favor the aggregation of deep convective clouds?. *Journal of the Atmospheric Sciences, EOR*, 3733–3745. https://doi.org/10.1175/JAS-D-18-0369.1

Silvers, L. G., Paynter, D., & Zhao, M. (2018). The diversity of cloud responses to twentieth century sea surface temperatures. *Geophysical Research Letters*, *45*, 391–400. https://doi.org/10.1002/2017GL075583

Silvers, L. G., Stevens, B., Mauritsen, T., & Giorgetta, M. (2016). Radiative convective equilibrium as a framework for studying the interaction between convection and its large-scale environment. *Journal of Advances in Modeling Earth Systems*, *8*, 1330–1344. https://doi.org/10.1002/2016MS000629

Slingo, A., & Slingo, J. M. (1988). The response of a general circulation model to cloud longwave radiative forcing. I: Introduction and initial experiments. *Quarterly Journal of the Royal Meteorological Society*, *114*(482), 1027–1062. https://doi.org/10.1002/qj.49711448209

Sobel, A. H., Bretherton, C. S., Gildor, H., & Peters, M. E. (2004). *Convection, cloud-radiative feedbacks and thermodynamic ocean coupling in simple models of the walker circulation* (No. 147). American Geophysical Union.

Stevens, B., Bony, S., & Webb, M. (2012). *Clouds on-off klimate intercomparison experiment (cookie) (Tech. Rep.)*. Retrieved from https://www.euclipse.eu/downloads/Cookie.pdf

Tiedtke, M. (1993). Representation of clouds in large-scale models. *Monthly Weather Review*, *121*(11), 3040–3061. https://doi.org/10.1175/1520-0493(1993)121⟨3040:ROCILS⟩2.0.CO;2

Tompkins, A. M. (2001). On the relationship between tropical convection and sea surface temperature. *Journal of Climate*, *14*(5), 633–637. https://doi.org/10.1175/1520-0442(2001)014⟨0633:OTRBTC⟩2.0.CO;2

Watanabe, M., Kamae, Y., Shiogama, H., DeAngelis, A. M., & Suzuki, K. (2018). Low clouds link equilibrium climate sensitivity to hydrological sensitivity. *Nature Climate Change*, *8*(10), 901–906. https://doi.org/10.1038/s41558-018-0272-0

Webb, M. J., Andrews, T., Bodas-Salcedo, A., Bony, S., Bretherton, C. S., Chadwick, R., et al. (2017). The cloud feedback model intercomparison project (CFMIP) contribution to CMIP6. *Geoscientific Model Development*, *10*, 359–384. https://doi.org/10.5194/gmd-10-359-2017

Wing, A. A., & Emanuel, K. A. (2014). Physical mechanisms controlling self-aggregation of convection in idealized numerical modeling simulations. *Journal of Advances in Modeling Earth Systems*, *6*(1), 59–74. https://doi.org/10.1002/2013MS000269

Wing, A. A., Stauffer, C. L., Becker, T., Reed, K. A., Ahn, M.-S., Arnold, N. P., et al. (2020). Clouds and convective self-aggregation in a multi-model ensemble of radiative-convective equilibrium simulations. *Journal of Advances in Modeling Earth Systems*, *12*(9), e2020MS002138. Retrieved from https://agupubs.onlinelibrary.wiley.com/doi/abs/10.1029/2020MS002138; https://doi.org/10.1029/2020MS002138

Wofsy, J., & Kuang, Z. (2012). Cloud-resolving model simulations and a simple model of an idealized Walker cell. *Journal of Climate*, *25*(23), 8090–8107. https://doi.org/10.1175/JCLI-D-11-00692.1

Zhao, M., Golaz, J.-C., Held, I. M., Guo, H., Balaji, V., Benson, R., et al. (2018a). The gfdl global atmosphere and land model AM4.0/LM4.0: 1. simulation characteristics with prescribed SSTs. *Journal of Advances in Modeling Earth Systems*, *10*(3), 691–734. https://doi.org/10.1002/2017MS001208

Zhao, M., Golaz, J.-C., Held, I. M., Guo, H., Balaji, V., Benson, R., et al. (2018b). The gfdl global atmosphere and land model AM4.0/LM4.0: 2. model description, sensitivity studies, and tuning strategies. *Journal of Advances in Modeling Earth Systems*, *10*(3), 735–769. https://doi.org/10.1002/2017MS001209

Zhou, C., Zelinka, M. D., & Klein, S. A. (2016). Impact of decadal cloud variations on the Earth's energy budget. *Nature Geoscience*, *9*, 871–874. https://doi.org/10.1038/ngeo2828